



UNIVERSIDADE D
COIMBRA

Lucas Eduardo Vieira Bottaro

ASSESSMENT OF THE DISPLACEMENTS AND
DEFORMATION MECHANISMS IN A ROCKFILL DAM
CASE STUDY OF CERRO DA MINA RESERVOIR

Dissertação no âmbito do Mestrado em Mecânica dos Solos e Engenharia Geotécnica, orientada pelo Professor Doutor Paulo José da Venda Oliveira e apresentada ao Departamento de Engenharia Civil da Faculdade de Ciências e Tecnologia da Universidade de Coimbra.

Janeiro de 2021

Faculdade de Ciências e Tecnologia da Universidade de Coimbra
Departamento de Engenharia Civil

Lucas Eduardo Vieira Bottaro

ASSESSMENT OF THE DISPLACEMENT AND DEFORMATION MECHANISMS OF A ROCKFILL DAM CASE STUDY OF CERRO DA MINA RESERVOIR

Dissertação no âmbito do Mestrado em Mecânica dos Solos e Engenharia Geotécnica,
orientada pelo Professor Doutor Paulo José da Venda Oliveira

Esta Dissertação é da exclusiva responsabilidade do seu autor. O Departamento de Engenharia Civil da FCTUC
declina qualquer responsabilidade, legal ou outra, em relação a erros ou omissões que possa conter.

Janeiro de 2021



UNIVERSIDADE D
COIMBRA

Acknowledgments

I would like to thank Somincor and Lundin Mining for the permission to use the data presented in this dissertation, and TPF Consultores, for presenting the problem and the opportunity to develop the study.

I would like to thank my advisor, Professor Dr. Paulo José da Venda Oliveira, for the guidance and patience during the development of this study. I extend my appreciation to all professors in the Department of Civil Engineering of the University of Coimbra, especially Professor Dr. Jorge Almeida e Sousa, who affected my trajectory in such a positive way.

I must express all my gratitude and love to the most important people in my life: my wife, for supporting me in every possible way, *e meus pais, pelo extraordinário exemplo.*

Abstract

Reservatório Cerro da Mina is an industrial water reservoir, part of Neves-Corvo mining compound, in the south of Portugal. Covered by an upstream impervious HDPE membrane and constructed approximately half on rockfill embankment and half on excavated rock, this dam experienced three moments of abrupt settlements on its embankments in the first years of operation. This behaviour raised concerns regarding the nature of the movements and the possibility of unanticipated problems. The analysis of the data from nine extensometers and one inclinometer installed in the highest section of the rockfill embankment, along with the assessment of the environmental conditions in the periods of interest, revealed that these significant unexpected vertical displacements coincided with periods of intense rainfall and rise in the water level in the reservoir. Both vertical and horizontal deformations of the rockfill showed a tendency of sudden increase when a new maximum in the precipitation record occurred. This represents an indication that the increase in humidity in the rockfill voids led to a significant decrease in the rock pore suction, causing wet-induced collapses in the rockfill. Additionally, the influence of the oscillation of the water level in the reservoir was estimated very small in the vertical direction, rejecting this factor as a major source of settlements in the rockfill. Long-term vertical deformation rates in the rockfill were calculated and presented a tendency fairly similar to what is expected for the kind of construction, showing no evidences of problems in that matter.

Keywords: rockfill dam; rockfill deformations; wet-induced collapse; time-dependent deformations.

Resumo

Reservatório Cerro da Mina é um reservatório de águas industriais, parte do complexo mineiro de Neves-Corvo, ao sul de Portugal. Impermeabilizado a montante por uma membrana de PEAD e construído aproximadamente metade em enrocamento e metade em rocha escavada, esta barragem esteve sujeita a três momentos de assentamento abruptos no aterro nos seus primeiros anos de operação. Este comportamento levantou questões acerca da natureza dos movimentos e da possibilidade de algum problema inesperado. A análise dos dados de nove extensómetros e de um inclinómetro instalados na secção de maior altura do enrocamento, juntamente com a avaliação das condições ambientais nos períodos em causa, revelaram que os deslocamentos significativos e inesperados coincidiram com períodos de intensa pluviosidade e subida no nível de água no reservatório. Tanto as deformações verticais como as horizontais apresentaram tendência de aumento acelerado sempre que um novo máximo no histórico de precipitações era registrado. O comportamento observado sugere que o aumento da humidade nos vazios do enrocamento gera uma redução significativa nos valores de sucção nos poros dos elementos rochosos, causando colapsos induzidos por molhagem no enrocamento. Além disso, os dados de observação indicam uma reduzida influência da oscilação do nível de água no reservatório na direção vertical, descartando este fator como causa principal dos assentamentos no enrocamento. As taxas de deformações verticais a longo prazo foram calculadas e apresentaram tendência similar ao previsto para este tipo de estrutura, não demonstrando sinais de problema neste sentido.

Palavras-chave: barragem de enrocamento; deformações no enrocamento; colapso induzido por molhagem; deformações tempo-dependentes.

Table of contents

| | | |
|--------|--|----|
| 1. | Introduction | 1 |
| 1.1. | Contextualization and objectives..... | 1 |
| 1.2. | Layout of the dissertation | 1 |
| 2. | Literature review on rockfill works deformation | 3 |
| 2.1. | Deformation mechanisms of rockfill works | 3 |
| 2.2. | Wet-induced collapse | 5 |
| 2.3. | Crack propagation..... | 8 |
| 2.4. | Rockfill as an unsaturated material | 9 |
| 2.4.1. | Stress corrosion | 10 |
| 2.4.2. | Constitutive models | 14 |
| 2.5. | Time-dependent deformation in rockfill..... | 16 |
| 2.5.1. | Estimation of time-dependent settlements in concrete faced dams..... | 19 |
| 3. | Cerro da Mina Reservoir: main aspects of the structure | 21 |
| 3.1. | Geological and geotechnical aspects and embankment zoning..... | 23 |
| 3.2. | Rockfill characteristics | 25 |
| 3.3. | Instrumentation plan | 34 |
| 4. | Assessment of the monitoring results | 37 |
| 4.1. | Vertical displacements in the rockfill..... | 38 |
| 4.2. | Horizontal displacements in the rockfill..... | 47 |
| 4.3. | Time-dependent deformation in the rockfill..... | 51 |
| 5. | Conclusions | 62 |
| 5.1. | Summary and conclusions of the study | 62 |
| 5.2. | Final considerations..... | 64 |
| 5.3. | Recommendation for further analysis..... | 64 |
| | References | 66 |

1. Introduction

1.1. Contextualization and objectives

Reservatório Cerro da Mina (RCM) is an industrial water reservoir located in Castro Verde, Portugal, part of Neves-Corvo mining compound, operated by Somincor. The reservoir was constructed approximately half on excavated rock, half on rockfill embankment, and it is fully covered by an upstream impervious high-density polyethylene (HDPE) membrane. Since the end of the construction (in the beginning of 2014), RCM recorded, on the first years of operation, a few unexpected vertical movements on its rockfill embankment. Abrupt vertical displacements occurred in three different times since 2015, raising concerns regarding their nature and the possibility of being a sign of an unanticipated problem.

Analysis of the moments in which the displacements occurred indicated that they were coincident with periods of increase in the water level of the reservoir and intense rainfall. The relation between changes in the environmental conditions and larger deformation rates are common in geotechnical engineering. However, in this case, it was considered prudent to determine which mechanisms were responsible for those movements and evaluate if these settlements could be considered normal compared to other similar dams.

In this context, the main objective of this study is to bring a consistent understanding of the deformations recorded in RCM in the period between 2014 and 2020, by defining and explaining the mechanisms responsible for the settlements and assessing the deformation rates recorded.

1.2. Layout of the dissertation

In addition to this introductory chapter, the work presented in this dissertation is divided as follows:

Chapter 2 presents a literature review on rockfill works deformation. The review gives particular attention to wet-induced collapse and the mechanisms associated to it, including the perspective of the phenomenon from the unsaturated soil mechanics. Besides collapse induced by wetting, time-dependent deformation in rockfill is succinctly covered in this chapter, including an overview of the principles and estimations of long-term deformation rates.

Chapter 3 describes RCM, presenting an overview of the reservoir, including geological and geotechnical aspects of the structure, characterization of the rockfill used in the embankment and the instrumentation plan of the dam.

Chapter 4 presents the monitoring results of the highest section of the dam in the period of interest. The vertical and horizontal displacements are presented and discussed, along with their relations with the environmental condition. The possible deformations mechanisms involved are investigated, and explanations for the movements are developed based on the findings. The rates of long-term deformation are presented and compared to estimations existent on the literature.

Chapter 5 summarizes the main conclusions of the study, presents the final considerations and suggestions for future studies.

2. Literature review on rockfill works deformation

The use of rockfill as a construction material for dams started in the middle of the nineteenth century in California, and since then the use of rocks in embankments has increased significantly (Kovacevic, 1994). The main reasons for that growth are related to their mechanical features, such as deformability, capacity to absorb large seismic energy and adaptability to various foundation conditions (Kalantary *et al.*, 2013). In addition, the use of materials quarried from the vicinities of the construction site is often a less expensive solution, and rockfill consists of a suitable option in many cases. Nevertheless, due to the high permeability of the material, the imperviousness of the structure have to be secured by other elements. The method chosen for that, along with the location of this structure, is usually considered to categorize the dam. The United States Bureau of Reclamation (USBR) classifies rockfill dams in three different groups, according to the position of the impervious zone: central core, sloping core or upstream membrane (USBR, 1987).

Rockfill has proved being a feasible alternative for constructing dams in several cases. The behaviour of this material, however, is not so well investigated as other types of geomaterials, especially when compared to soils. Kalantary *et al.* (2013) suggest that the primary reason for that is the limitation of experimental apparatus suitable for testing rockfills. Large oedometers and triaxial cells are necessary to experiment this material, and most relevant research only occurred recently. On the other hand, a large volume of data regarding construction and operation of rockfill dams has been collected since the last century, and many studies have been conducted with these data. Therefore, the design of rockfill dams is still customarily based on empirical methods, relying on engineering judgment and experience (Fell *et al.*, 2015).

Nevertheless, in the last decades there has been significant development in understanding the stress-strain-strength relations in rockfill works (Kovacevic, 1994), allowing engineers to recognize, predict and assess the behaviour of a structure based on the knowledge of the mechanisms involved.

2.1. Deformation mechanisms of rockfill works

The use of rockfill in structures such as dams made necessary to develop a higher understand of the mechanisms influencing the strength and stiffness of this material. The importance of this kind of work made crucial to be able to predict how the structure will behave under the conditions imposed during construction, first filling, extreme rain events and other

circumstances present through its lifespan. It became necessary to pursue a rigorous knowledge of all the physical and chemical processes taking place in the structure, so the monitoring observations can be correctly interpreted, avoiding improper conclusions.

There is a limited number of mechanisms involved in the deformation of rockfill, although affected by many factors. These mechanisms can take place in each particle or in the contacts among them. Bulk deformation and particle breakage consist of intra-particle mechanisms. Rotation and slide of particles and contact crushing are considered interparticle displacements (Charles, 1990).

Bulk deformation consists of the deformation of the rock particle. Like any other materials, when under load, rock elements are susceptible to immediate and time-dependent deformations. Each particle in the granular mass will be subjected to stress and so will respond with strain, influencing the overall deformation of the mass. The amount of deformation due to this process is, however, reduced when compared to the other mechanisms. Particle breakage, on the other hand, plays a significant role on the overall deformation of rockfill. When the stress in a plane of the particle caused by the forces applied exceeds the strength along this plane, a breakage takes place, and a rock element breaks in two or more pieces. Consequently, the structure of the mass changes and a redistribution of forces occurs (Clements, 1981). Figure 2.1 shows rockfill particles breakage due to compression.



Figure 2.1 - Particle breakage in rockfill (Zhou and Song, 2016)

Considered an interparticle mechanism, contact crushing generally occurs in the edges of the rockfill elements. Each particle in the granular mass is subjected to forces when in contact with others, generating stress in the elements. This stress may be excessive in some peripheral zones, and crushing and / or spalling takes place until the forces are redistributed to larger contact areas and the stress is adequately accommodated. The movement of particles toward each other caused by contact crushing is a normal displacement in the contact plane. However, rotation and slide of particles relative to each other may occur as well, consisting thus in a tangential displacement. This movement is opposed by the friction among particles, and since the dynamic coefficient of friction is smaller than the static, once this movement starts it only stops when a more stable situation is reached, result of the distribution of forces. In some cases, these displacements also create crush or spalling as result (Clements, 1981).

It is, however, impossible to determine what is the exact contribution of each of the four mechanisms. In each situation, their influence is dependent of the load applied, rock properties, particle shape, void ratio, relative humidity (RH) and time. Oldecop & Alonso (2001) proposed a micromechanical conceptual model to explain how deformations occur in rockfill. In the first stages of compression, the main mechanism is rotation and slide of particles, inducing rearrangement in the structure. This causes the increase of the granular structure, till the point this process is blocked, and no further deformation can take place without the breakage of rock particles. When the breakage occurs, rearrangement of the rocks takes place again, and new equilibrium is reached. This is a continuous process, influenced by changes in stress state, variation of humidity and time. The following section succinctly describe how these factors impact the overall deformation of a rockfill work, with particular focus on the effect of humidity.

2.2. Wet-induced collapse

When first investigated, the settlements observed in rockfill works when wet under constant load were difficult to explain. Terzaghi (1960) suggested that the high stresses existent in the contacts between rocks induce the breakage of particles, and consequently the rockfill structure is rearranged. Many tests were conducted in the 1960s and 1970s, and the results of these experiments converged to the conclusion that particle breakage is in fact a primarily cause of the deformation of rockfill, and water plays an important role in this mechanism by weakening the parent rock (Charles, 1990).

The sudden deformation upon flooding of a soil or rockfill mass, conventionally termed wet-induced collapse, is a mechanism seen in rockfill dams for a long time, but not fully understood until a few decades ago. It often happens in the upstream shell of zoned rockfill dams during

the first impoundment, or in the downstream shell due to large rainfall events (Marsal *et al.*, 1976, and Naylor *et al.*, 1997, mentioned by Oldecop and Alonso 2001).

Many authors developed studies aimed to understand this phenomenon in the second half of the 20th century, including the relevant work of Nobari and Duncan (1972), in which they investigated the effects of wetting in the properties of rockfill. Their study revealed that the initial moisture content in the rockfill plays a very significant role in the amount of collapse resulting of the flooding of the specimen. The tests demonstrated an inverse relation between the initial humidity and the amount of axial deformation resultant of collapse. They also found that initially dry samples wetted upon load tend to present similar final void ratio of the samples wetted before loading. Figure 2.2 presents the results of axial compression tests for freshly broken greywacke and sandstone with maximum size of 3.8 cm.

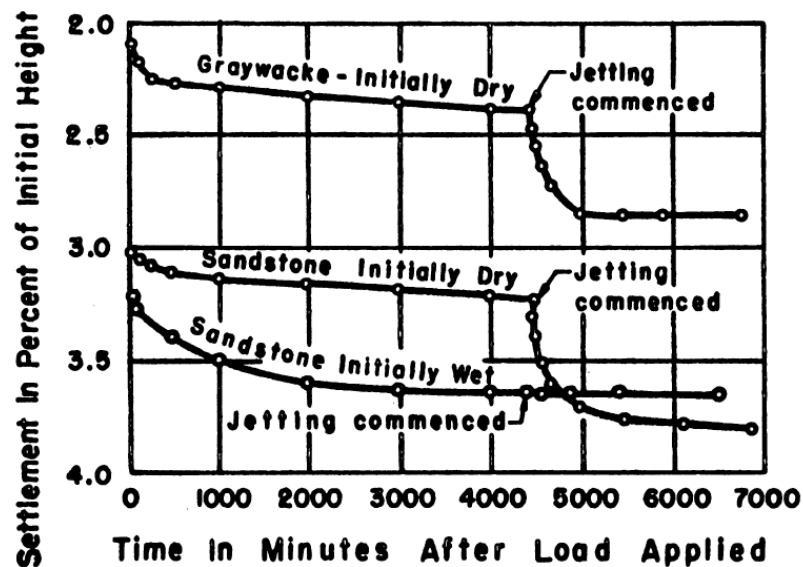


Figure 2.2 - Compression and collapse of rockfill material (Nobari and Duncan, 1972, after Sowers *et al.*, 1965).

In a review of the behaviour of Beliche Dam, a largely studied clay core rockfill dam in Portugal, Alonso *et al.* (2005) showed the relation between rain intensity and the rate of movement recorded in settlement plates. Justo and Duran (2000) also indicated that the same kind of behaviour has been observed in Martín Gonzalo Dam, a rockfill dam with an upstream impervious membrane in Spain. These two structures have recorded an acceleration of settlements during the first large rainfall events, however, after a certain period, these occurrences were not able to cause abrupt vertical movements anymore. Figure 2.3 and Figure

2.4 present the relation between rainfall intensity and settlements recorded in Beliche Dam and Martín Gonzalo Dam, respectively.

It is possible to notice in Figure 2.3 and Figure 2.4 that the early strong rainfall events caused significant settlement. After each collapse, it was necessary a larger occurrence to trigger a new strong vertical movement, until the point when collapses induced by wetting were not recorded anymore, despite the intensity of the rainfall. Alonso *et al.* (2005) states that once the rockfill reaches 100% of humidity for the first time, wetting collapse ceases. The theory supporting this mechanism will be discussed further in section 2.4.

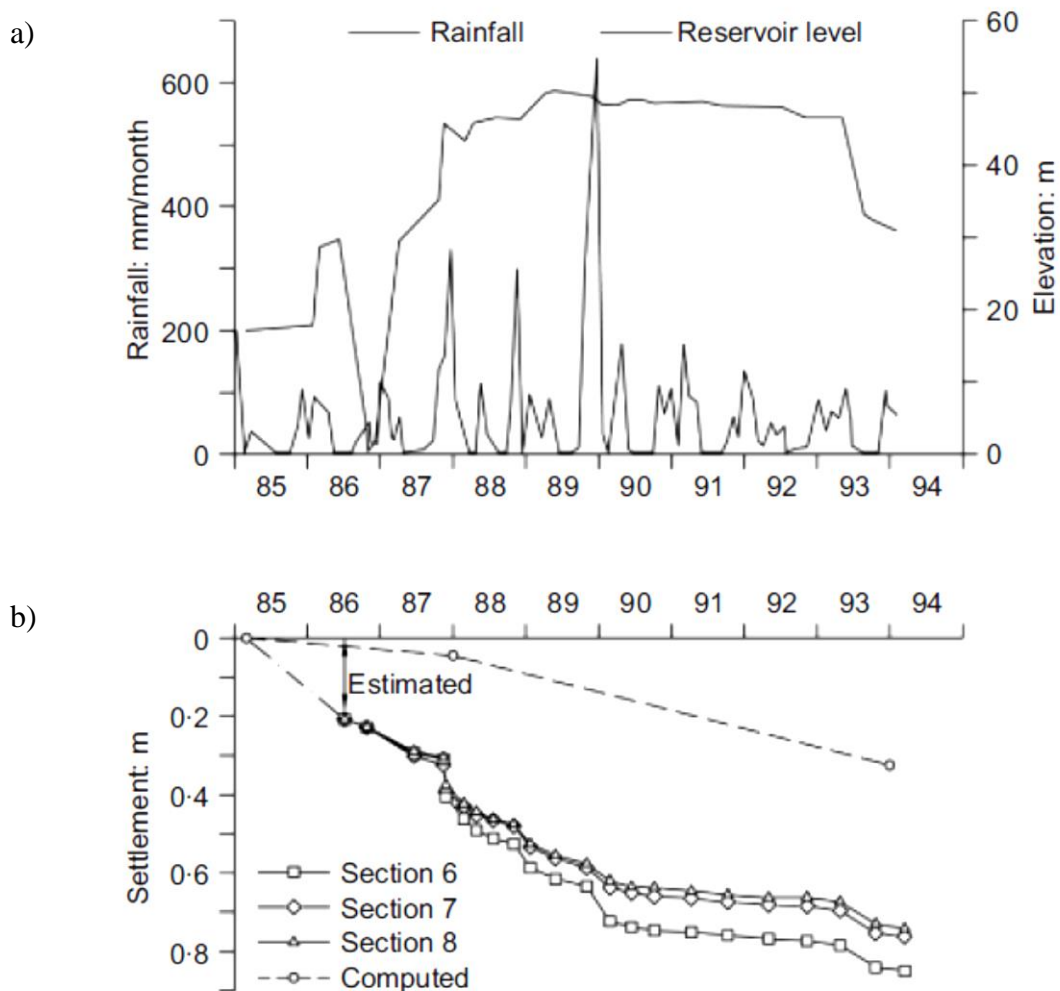


Figure 2.3 - Beliche Dam: a) rainfall intensity and reservoir level after dam construction and b) vertical settlements registered at crests mark and predictions by Naylor *et al.* 1997 (Alonso *et al.*, 2005, after Naylor *et al.*, 1997)

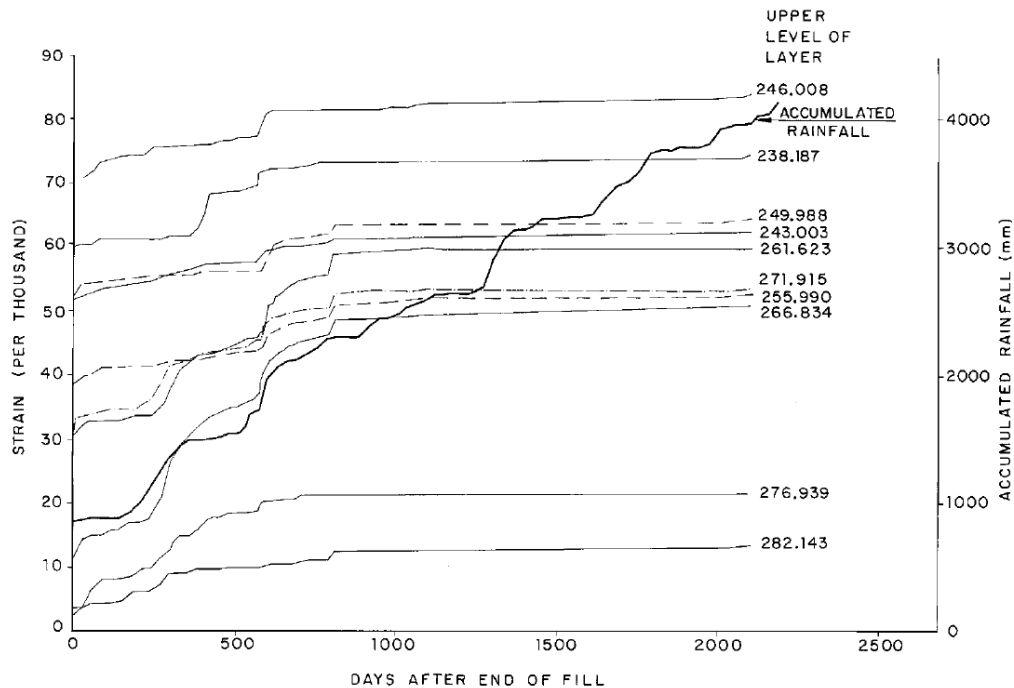


Figure 2.4 - Martín Gonzalo Dam: strain of the different layer at a settlement plates line at the highest section and accumulated rainfall after filling (Justo and Duran, 2000)

2.3. Crack propagation

It is relevant, at this point, to mention that rockfill is typically described as having two sets of voids. The first set, normally termed rockfill voids, consists of the large inter-particle spaces formed between the rockfill elements. The second set, usually referred as rock pores, exists in a much smaller scale, corresponding to the natural porosity of the rock particle. For engineering purposes, settlement relates directly to the reduction of the first set (rockfill voids), but for what the mechanism of particle breakage concerns, the second set (rock pores) plays a leading part, particularly the ones at the surface of the elements (Oldecop and Alonso, 2001).

The research of Nobari and Duncan (1972) revealed a pertinent aspect related to the grain size of the rocks. Sieve analyses conducted previously and after the tests showed variation in the samples, indicating that some fracture occurred in the rockfill. These findings corroborate with the proposal that particle breakage plays a key role in the settlement of rockfill dams. Oldecop and Alonso (2001) assert that it can be concluded from this and other similar experiments that particle breakage is indeed the most relevant phenomenon involved in the deformation of rockfill. Furthermore, Alonso and Tapias (2018), Xiao and Liu (2018), Zhou and Song (2016), Kermani (2016), among other authors, mention particle breakage as the main process

responsible for post-construction settlement in rockfill, including the reduction of void ratio in the rockfill after impoundment, when there is no significant variation in stress state caused by loading. This mechanism can be explained simply as the full propagation of a crack across a plane of the particle. The central question is to understand how this propagation occurs, and which factors have most influence in it.

Larger particles, such as the elements present in a rockfill work, are expected to have more flaws in comparison to smaller grains. In addition, larger contact forces are anticipated as well, and the more angular the element the more stress concentrates in the vertices (Alaei and Mahboubi, 2012). These characteristics make rockfill elements much more propense to present cracks – at the particle level – than sand or fine-grained soils, and this is fundamental to understand the different behaviour of rockfill when examining deformation.

Crack propagation ultimately causes rock particle to break, leading to a rearrangement of the rockfill structure, until a new equilibrium is finally achieved. Each rearrangement induces a macroscopic strain increment, and according to Oldecop and Alonso (2007), when the blockage of the granular structure is reached, the deformation process of the rockfill becomes controlled by a phenomenon named stress corrosion.

2.4. Rockfill as an unsaturated material

Materials used for the construction of dams are compacted and therefore can be thought, in a broad sense, as unsaturated materials. According to Alonso and Cardoso (2010), the different types of geotechnical materials under unsaturated conditions must be distinguished. It is usual to categorize these materials as: rockfill, sands and granular materials, regular compacted soils, compacted soft rocks, and cemented materials. These authors state that this separation is not only due to where they are found in the granulometric scale but, because they have very particular behaviours, they differ in the mechanisms involved in their deformation, which are associated to the state of the water in the voids. Also, the sort of information provided by grain size is very limited, since unsaturated soil mechanics deals with the air and water in the pores, and thus pore size distribution would be a more useful measurement.

The role of suction in the behaviour of fine-grained soils is reasonably long known and well understood by the soil mechanics of unsaturated soils. Granular soils (as coarser sands and gravels) are less sensible to changes in water content, and the reasons are also properly understood for many decades. On the other hand, although the effects that wetting have on rockfill embankments has been recorded for a long time, the understanding of the role of relative

humidity in the mechanisms involved are reasonably recent. Alonso and Cardoso (2010) explain this new mechanism, exclusively found in rockfill:

“It turns out that the relative humidity (or, alternatively the total suction) of the “atmosphere” filling the large voids between rockfill particles controls the stiffness of coarse grained materials. This is an interesting result because water suction maintains a key role for volumetric changes at the large scale, but the basic deformation mechanism is now totally different. Oldecop and Alonso (2001) indicated that the role of the total suction is to control the speed of crack propagation within individual rockfill particles. This is a “new” mechanism, not present in soils. It is as if water would act as a corrosive agent (...). The deformations observed in these materials are therefore related with structural changes caused by the rearrangement of the fragments resulting from a breakage process.” – Alonso and Cardoso (2010).

As stated in the previous paragraph, the combined action of water and applied stress enables a reaction that takes place at the crack tip. This phenomenon is named stress corrosion and its rate defines the velocity in which a crack propagates. Rockfill deformation is, therefore, dependent on relative humidity, time and, as expected, the stress state.

2.4.1. Stress corrosion

In this process of stress corrosion, the reaction between the rock and the water filling the crack is boosted by the stress at the crack tip. Figure 2.5 shows a schematic representation of stress acting in a rockfill element. The stress intensity factor K , which in linear elastic fracture mechanics is defined by Equation (1), characterises the stress state in the crack tip zone (Tapias *et al.*, 2015, after Broek, 1986).

$$K_i = \beta_i \sigma_i^* \sqrt{\pi a_i} \quad (1)$$

where σ_i^* is the stress that would act across the plane of crack i if the particle was not cracked; a_i is the half-length of crack i ; and β_i is a non-dimensional factor that encompasses other factors, representing the geometry of the particle, position of the crack, direction and point of application of loads and relative size of the crack in relation to the particle size. For the most common geometries, the factor β_i can be found in handbooks (Oldecop and Alonso, 2001, after Murakami, 1987).

The local stress σ_i^* is dependent on the macroscopic stress, shown in Figure 2.5 by means of principal stresses. Therefore, it is expected that when the applied load increases, the local stress and consequently the stress intensity factor increases as well.

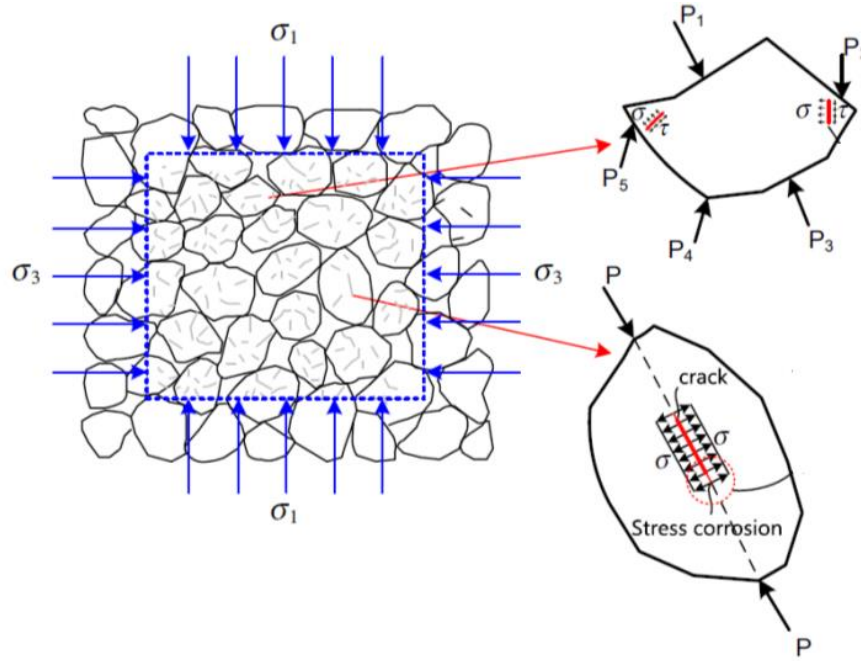


Figure 2.5 - Stress acting in a rockfill element (adapted from Zhou and Song, 2016).

There are two very significant values of the stress intensity factor. The first one is the fracture toughness K^C , that can be interpreted as the value in which crack propagates suddenly and the element containing the crack collapses instantaneously. The other value is the stress corrosion limit K^0 , that represents the threshold for which the crack starts to propagate, i.e., for values of K smaller than K^0 the corrosion reaction does not occur and the crack will not increase at all. The value of K^C can be considered, with some limitations, material properties. K^0 is influenced by the RH in the voids of the rockfill. For values of K in the interval of K^C and K^0 , the crack will propagate with a velocity V , defined by Equation (2) propose by Charles (1958) (Tapias *et al.*, 2015).

$$V = V_0 \left(\frac{K}{K^C} \right)^n \quad (2)$$

where V_0 and n are normally obtained by fitting experimental data. The parameter n is dependent on relative humidity, giving higher values for drier conditions. It is important to state that this model is purely phenomenological, with no physico-chemical fundament in the equation (Oldecop and Alonso, 2007).

Stress corrosion experiments are usually conducted under constant suction conditions, and the data are often plotted in a crack velocity versus stress intensity factor graph for each value of RH. The typical curve shape is presented in Figure 2.6, in a model suggested by Oldecop and Alonso (2001).

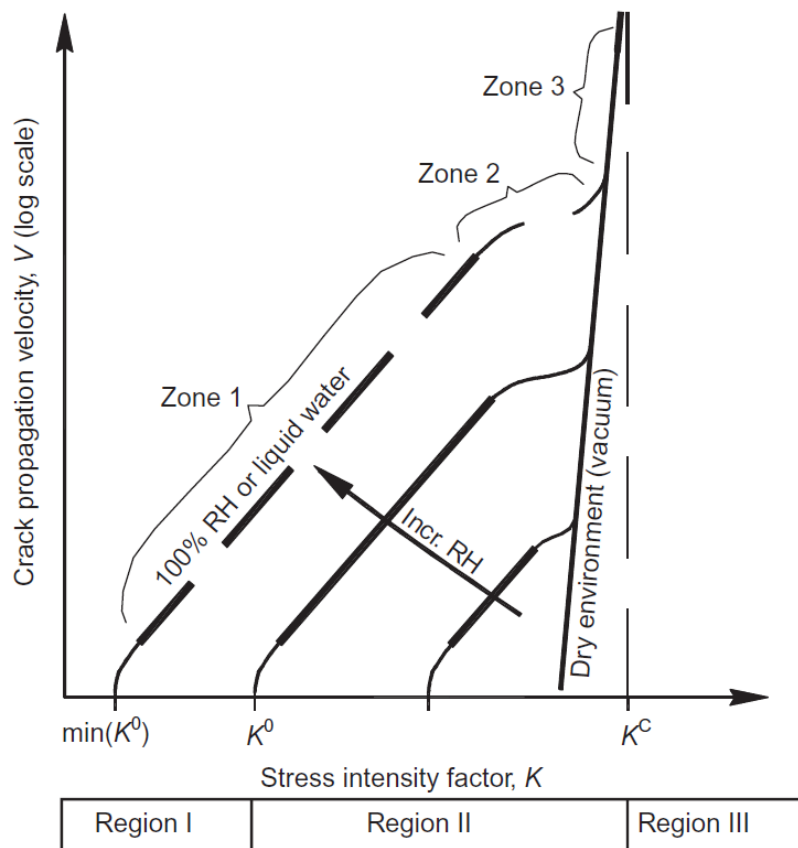


Figure 2.6 - Schematic stress corrosion curves and conceptual model proposed by Oldecop and Alonso (2001) (Oldecop and Alonso, 2007).

The influence of suction in the rockfill voids might be seen in Figure 2.6, as the curve representing Equation (2) moves to the left with the increase of RH. Not only the value of K^0 reduces, which means cracks are able to propagate under a reduced stress state, but for the same value of K , or same stress state, the propagation velocity increases with the growth of relative humidity. Figure 2.7 presents several results of stress corrosion from experimental data published by Atkinson (1984) and Wiederhorn (1982) and compiled by Oldecop and Alonso (2007). It is possible to observe the relation between crack propagation velocity and stress intensity factor for different types of materials and the plotted curves of the model proposed by Charles (1958) for $V_0 = 0,1$ m/s.

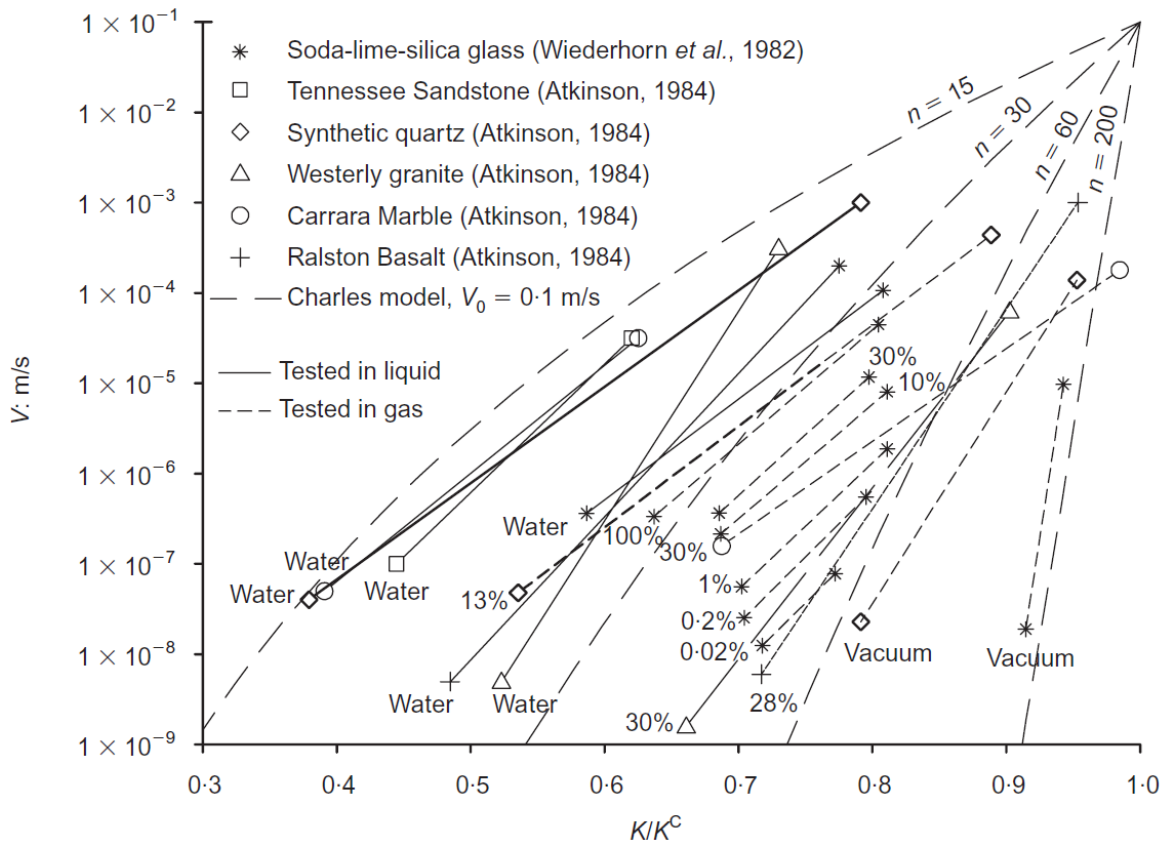


Figure 2.7 - Stress corrosion experimental data and plots of Charles model considering $V_0 = 0,1\text{m/s}$. Testing condition indicated next to each curve: immersed in liquid water, controlled relative humidity (in %) or vacuum (compiled by Oldecop and Alonso, 2007).

It is possible to see in Figure 2.7 that the tendency of the curves obtained by experimental data fits the theoretical solution, at least for zone 1 (as defined in Figure 2.6). This similarity suggests that cracks propagate in zone 1 as a result of the mechanism proposed. In zone 2, propagation velocity becomes almost constant, and Oldecop and Alonso (2007) suggest that the diffusion of water vapour along the crack controls the mechanism. The same authors state that in zone 3 propagation occurs in a velocity so intense that the water cannot reach the tip of the crack, and thus RH does not have influence.

Variations in the water content in the voids of the rockfill is normally affected by the rise of the water level in the reservoir or intense rainfall events, although Gallipoli et al. (2003) demonstrated that the degree of saturation also change during shearing, even at constant suction and constant mean net stress. This phenomenon is related to the change in the void ratio of the macro structure caused by shear. Since particle breakage leads to the rearrangement of the structure and consequently reduction of the void ratio of the macro structure, it is reasonable to

think particle breakage as a progressive iterative process. The relation between shear and humidity, however, is not limited to the variation in the voids and consequently suction. As clarified in this section, water alters the strength of the rock, and this has a direct effect in the properties of the rockfill when subject to shearing.

Marsal (1967), Charles and Watts (1980) and De Mello (1977), mentioned by Alonso and Cardoso (2010), showed that the strength envelope of rockfill is curved, especially for low stress levels. De Mello (1977) proposed the following equation,

$$\tau_f = A(\sigma)^b \quad (3)$$

in which A and b are coefficients defined empirically. The nonlinearity is due to particle breakage when shear and compression occurs. In addition to nonlinearity, the strength envelope is also dependent on suction. Rocks more susceptible to particle breakage, such as schists and shale, have a more marked dependence on relative humidity than tough rocks with isotropic properties, like limestone (Alonso and Cardoso, 2010).

2.4.2. Constitutive models

It is not the aim of this study to make a review of constitutive models for rockfill, since it is an extensive and very complex issue, and could not be properly covered in the scope of this dissertation. But a brief look on this matter can help understanding how rockfill behaves under the variation in relative humidity, especially through the stress space $p' \times q \times s$, where p' is the mean effective stress, q is the deviatoric stress and s represents the suction in the rockfill. Most of the models used to characterize rockfill behaviour are linear elastic and nonlinear elastic (Varadarajan et al., 2006). Recently, elastoplastic constitutive models have been proposed to describe the behaviour of rockfill. Alonso et al. (1990) proposed the largely known Barcelona Basic Model (BBM), suitable for partially saturated soils. Oldecop and Alonso (2001) suggested a model for rockfill compressibility. Despite the differences between unsaturated soils and rockfill, relevant similarities can be found in their behaviour, such as the decrease of compressibility with the increase of suction.

BBM originally had an isotropic formulation, but it was extended to triaxial states by means of ellipses that span in the p axis. Like any other constitutive model, it has several limitations, including all existent in the modified cam-clay model (Alonso and Cardoso, 2010). Despite that, analysing the yield surface can bring a better understanding of the collapse of rockfill due to wetting. Figure 2.8 illustrates a three-dimensional view of the yield surface in (p, q, s) stress space, according to Alonso et al. (1990).

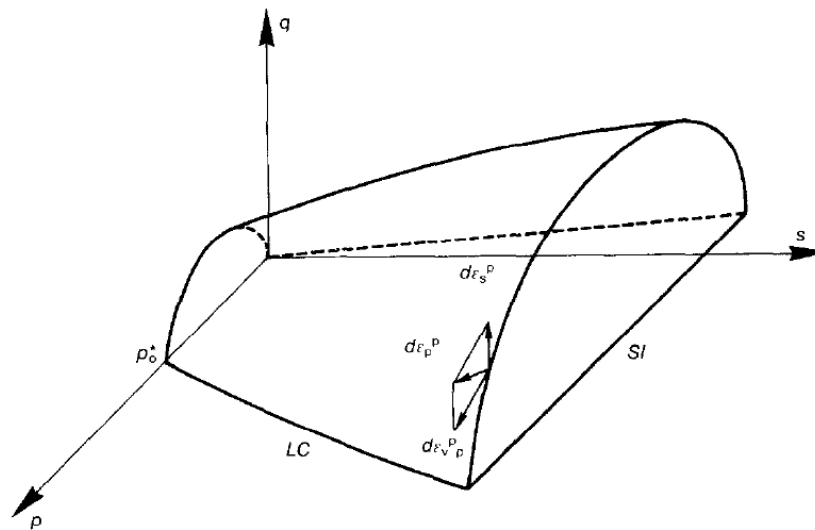


Figure 2.8 - Three-dimensional view of the yield surface in (p, q, s) stress space (Alonso et al., 1990)

As it can be seen in Figure 2.8, the yield surface enlarges with the increase of suction. It means that, for the same mean and deviatoric stresses, an increase in load could cause elastic or plastic deformations, or both, depending on the relative humidity present in the rockfill voids. This illustration is very helpful to understand wetting collapse.

Taking as example an element in a rockfill dam, with a hypothetical stress state located on the yield surface and subject to a high value of suction, as depicted in Figure 2.9. If a variation in relative humidity occurs due to an intense rainfall event, for example, and the load remains unchanged, the stress point representing that element will move parallel to the suction (s) axis towards its new location, closer to the origin. It means that this point suddenly shifts to a plane in which the yield surface was smaller than the one for the previously amount of suction, causing abrupt plastic deformation to cope with this, and thus the material hardens and form a new, enlarged yield surface. That abrupt plastic deformation is the wetting collapse.

Figure 2.9 also helps to understand why new collapses are only expected when suction reaches a new historical minimum. As the variations in suction above this value would make the stress point move below the yield surface, no sudden deformation is anticipated. Therefore, after full saturation of the rockfill voids once happens, no wetting collapse is expected, since every change in suction would make the stress point move underneath the yield surface.

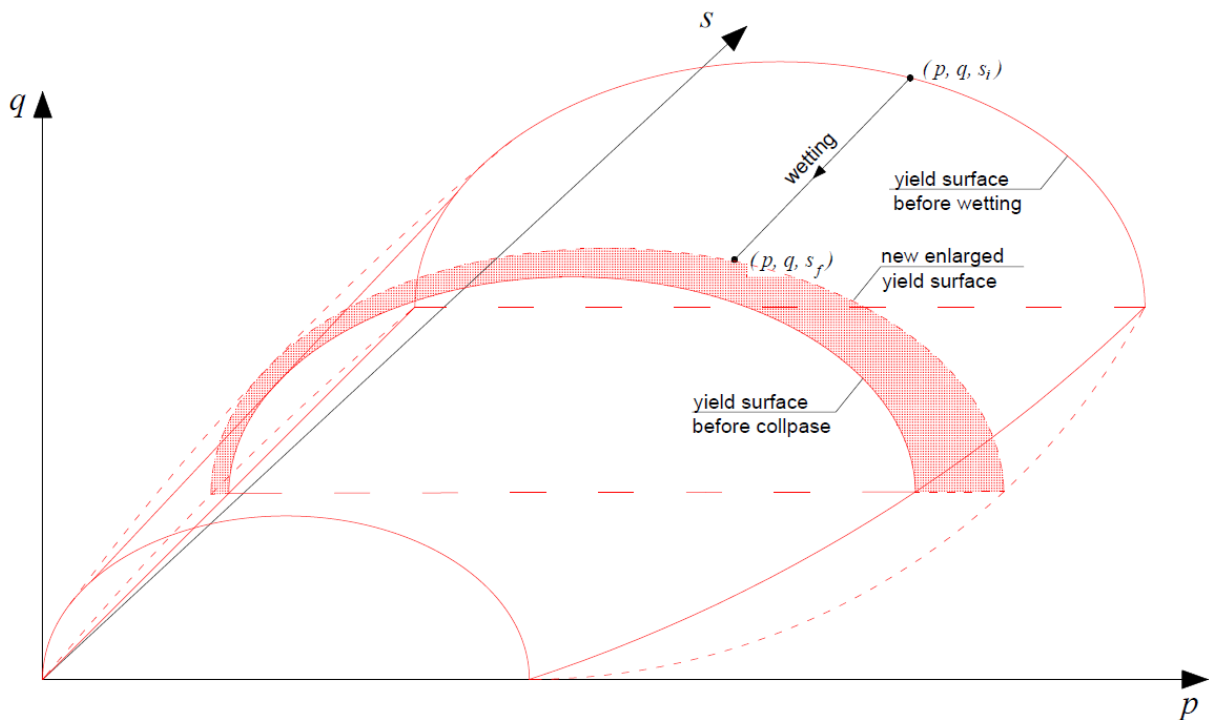


Figure 2.9 - Yielding behaviour of an element subject to wetting.

Suction, however, is not the only factor that affects the particle breakage. Oldecop and Alonso (2001) proposed 3 stages for increase in stress levels, limited by 2 thresholds: yield stress and clastic yield stress. For stress levels below yield stress, only accommodation of fragments occurs, and the material is subject to elastic deformation. When stress levels reach values above the yield stress, but smaller than clastic yield stress, deformations occur due to particle rearrangement, and the rockfill is subject to plastic strains. For stress levels that surpasses clastic yield stress, more breakage and crushing will take place, and consequently also more readjustment. Clastic yield stress is defined, therefore, as the threshold for which particles will break (Alonso and Cardoso, 2010). It is important to notice that deformations related to the stress levels higher than the yield stress are plastic, but the slope of the virgin compression curve increases when clastic yield stress is achieved.

2.5. Time-dependent deformation in rockfill

Like any other geotechnical material, rockfill is susceptible to long-term deformations. A time-dependent breakage of the particles under constant load follows the same principles described in the previous sections: the delayed fracture of rockfill elements generates smaller fragments, which fill the voids more efficiently, enhancing densification and thus causing settlements.

These macroscopic observations can be explained by the same phenomenon, based on crack propagation induced by stress corrosion mechanisms (Oldecop and Alonso, 2007).

According to Alonso and Tapias (2009), long-term deformation mechanism is a consequence of the crack propagation velocity in particles, as demonstrated in their experimental study. Large oedometer tests and field observation demonstrated that, when under constant humidity conditions, creep deformations in rockfill are linearly related to the logarithm of time. Figure 2.10 presents the results of secondary deformation on limestone gravel under a suction controlled oedometer test.

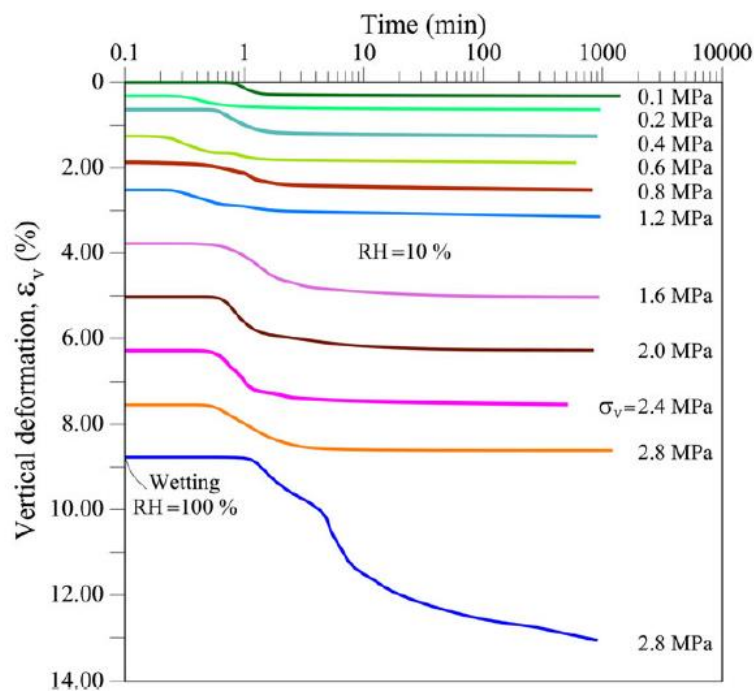


Figure 2.10 - Time-deformation records of rockfill tested in a suction controlled oedometer (Alonso and Tapias, 2009, after Ortega, 2008).

This process has been responsible for relevant crest settlements in several dams, as depicted in Figure 2.11, where Oldecop and Alonso (2007) compiled the results observed in many structures. It is also possible to notice the correlation between construction method and time-dependent deformation rates. According to the characteristics of the structure, creep settlements in the rockfill may be more relevant or less relevant for the safety or performance of the construction. However, that is not commonly a very concerning issue in dams, although there were a few cases relating to service limit state problems in history (Cetin *et al.*, 2000).

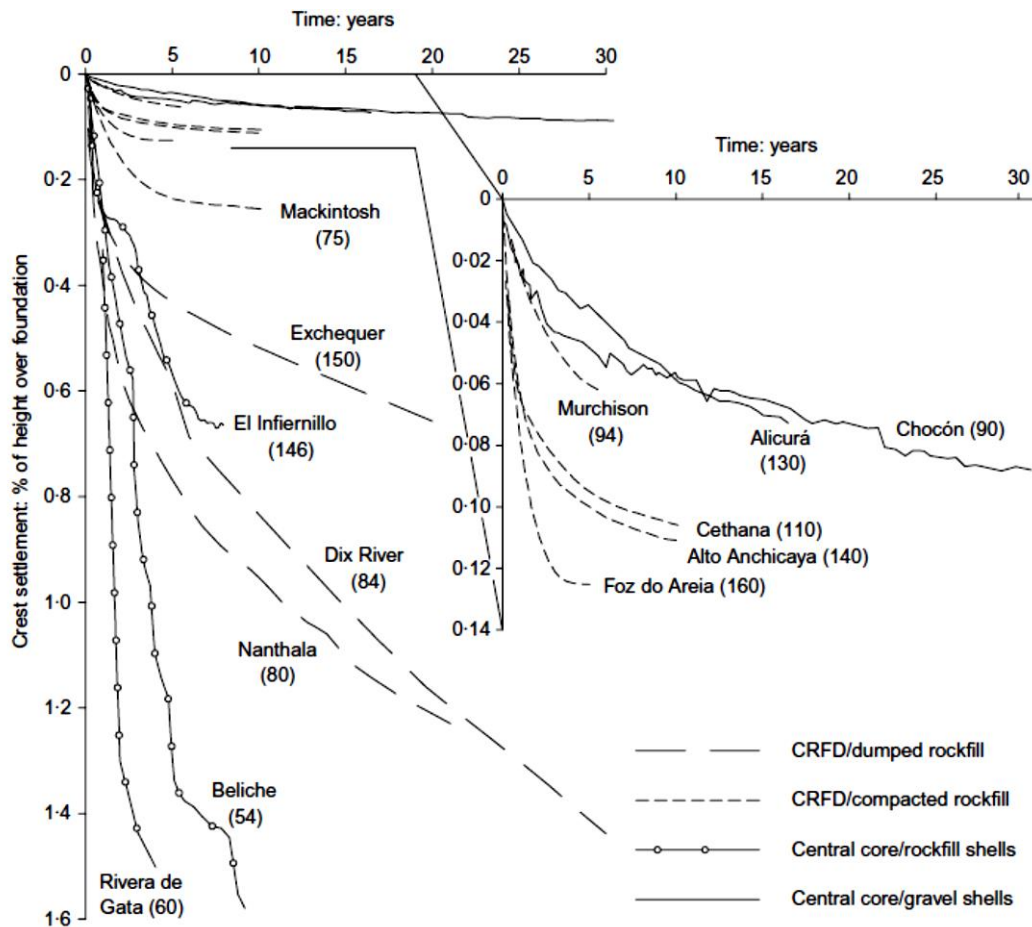


Figure 2.11 - Record of crest settlements of rockfill dams built in the 20th century. Name of the dam (height in m) next to each curve. Data sources: Marsal et al., 1976; Sherard & Cooke, 1987; Soriano et al., 1992; Naylor et al., 1997. (Oldecop and Alonso, 2007).

A very important aspect about time-dependent deformations is that creep is in general superposed with strains due to other mechanisms caused by different phenomena, such as wetting collapse, repeated loading or earthquakes. Normally, these other processes have considerably more influence in the dam performance than creep (Oldecop and Alonso, 2007). Another relevant problem when analyzing time-dependent deformation is the scale effect on creep. Rockfill often consists of particles that are alone bigger than common testing equipment, in many cases having elements as large as 1m or more. Due to the small size of testing equipment available in laboratories (when compared to rockfill elements), test samples must use reduced size particles. Until the scale effect is fully understood, these results must be considered cautiously for practical engineering purposes (Zhou and Song, 2016).

2.5.1. Estimation of time-dependent settlements in concrete faced dams

Hunter and Fell (2002) suggest a method to estimate long-term settlements in concrete faced rockfill dams based on the analysis of the 35 dams, according to the authors “with good quality information on construction materials and placement methods, and good quality internal and surface settlement monitoring records”. The authors concluded that time-dependent settlements in rockfill dams is, as observed in laboratory tests, linearly related to the logarithm of time, especially when taking into consideration larger periods, for example 10 to 30 years after the end of construction.

Figure 2.12 shows the relation between long-term rate of crest settlement and embankment height. Extremely high strength rock and gravel, high strength rock and medium strength rock are plotted in the graph. As aforementioned, this method is purely empirical, and although it consists in a valid reference for estimation and comparison for monitoring records, it shall be used with cautious and engineering judgement, since there are some other factors that could influence post-construction deformation.

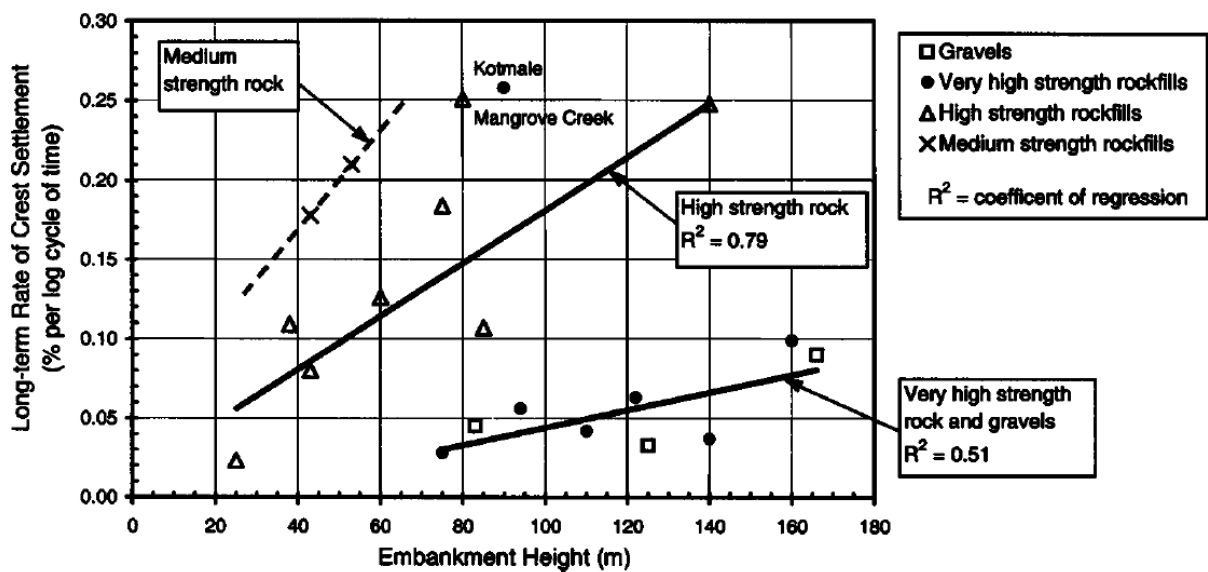


Figure 2.12 - Long-term crest settlement rates versus embankment height for compacted rockfill dams (Hunter and Fell, 2002).

It is possible to notice in Figure 2.12 that long-term settlement rate in rockfill dams with impervious faces is significantly related to the strength of the rock matrix and the embankment’s height. Hunter and Fell (2002) also mention other factors that may increase time-dependent

deformation, such as large fluctuations in the reservoir levels, significant leakage to the embankment, use of weathered rockfill or high rainfall rates.

Kermani (2016) presents a similar study, that essentially differs regarding when the time-datum should be set. Unlike Hunter and Fell (2002), which consider day zero as the end of the construction, Kermani (2016) suggests that it would be more appropriate to establish the beginning of the counting when the impoundment is completed, since relevant plastic deformations and changes in the stress state in the rockfill occur in that phase. This proposal follows the same concept used for oedometer tests with load increment, in which time is reset every new stage. A slightly different graph from the one developed by Hunter and Fell (2002) is presented by Kermani (2016), as depicted in Figure 2.13.

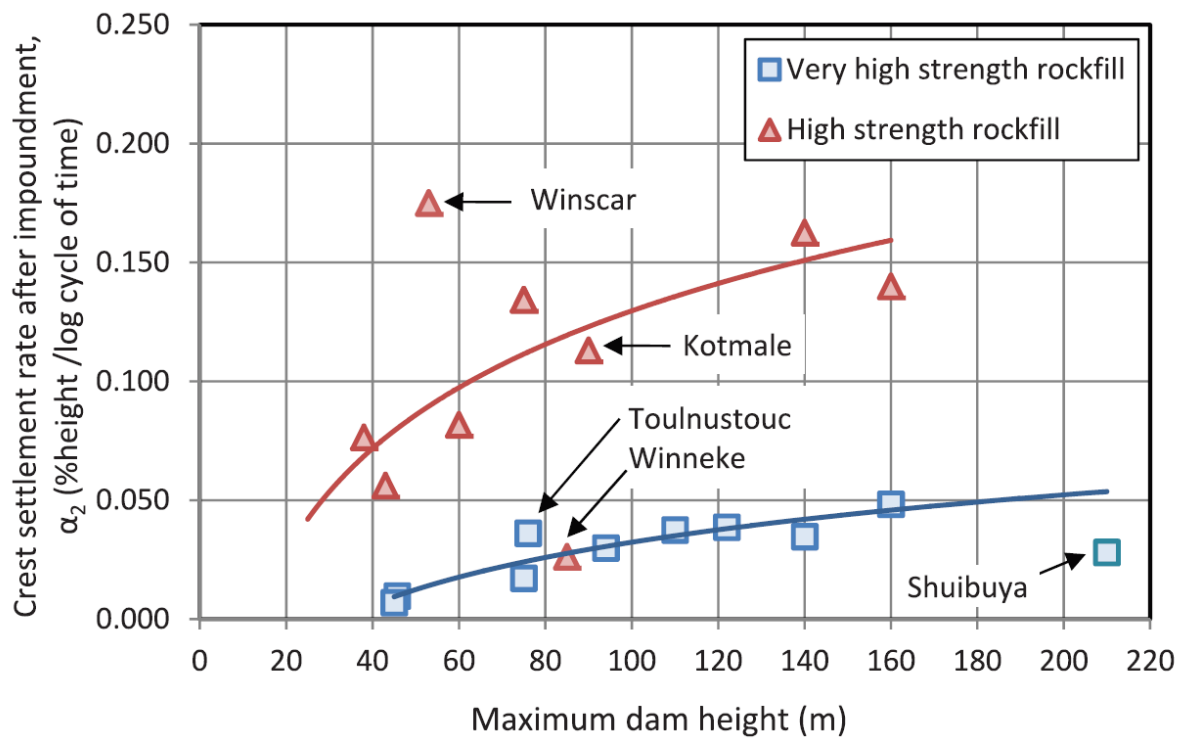


Figure 2.13 - Long-term crest settlement rates after impoundment versus embankment height for compacted rockfill dams (Kermani, 2016).

3. Cerro da Mina Reservoir: main aspects of the structure

RCM is an industrial water reservoir with 1 450 000 m³ of storage capacity, part of the Neves-Corvo mining compound, the largest underground copper-zinc mine currently in service in Portugal. Located in the city of Castro Verde, in the south of Portugal (37,56° N; 7,95° W), this world-class mine has been operating since 1988 by Somincor, a subsidiary of Lundin Mining Corporation, from Canada (Ferreira et al., 2018).

Since the operation started, the tailings produced in the mining process, which have a very high acid generation potential, have been stored sub-aqueously in Cerro do Lobo Tailings Management Facility (IRCL). This pond also stores water from the ore processing plants, and after two decades of operation, this facility was close to its maximum capacity. Concomitantly, the discovery of a new ore deposit required a change in the tailings' disposal process. The new method significantly reduced the capacity of IRCL to store industrial water, and thus the construction of a new facility – RCM – was necessary (Tavares et al., 2011, Ferreira et al., 2018). The location of Neves-Corvo Mine, RCM and IRCL are presented in Figure 3.1, and a panoramic view of RCM is shown in Figure 3.2.



Figure 3.1 - Cerro da Mina Reservoir and Cerro do Lobo Tailings Management Facility (Google Earth, 2020).



Figure 3.2 - Aerial view of Cerro da Mina Reservoir (Teixeira Duarte, 2010).

Cerro da Mina Reservoir is limited at north and west by a rockfill embankment, and at east and south by excavated rock, as represented in Figure 3.3. At elevation 240 m, the crest is 1270 m long, approximately half on embankment, half on excavated slope. The embankment consists, on the west side, of a main embankment with a maximum height of approximately 30 m, and on the north side, of a saddle embankment of 11 m on its highest section, both with an inclination of 1V:2H on their upstream and downstream faces. The excavated slopes are 1V:1,5H and have a maximum height of 21 m (Tavares et al., 2011).

Due to chemical activity of the industrial water stored, the reservoir is operated considering zero discharge to the environment. A double lining HDPE membrane of 2,5 mm was designed to waterproof the pond, lying on a geocomposite clay liner. To control any eventual seepage beneath the reservoir, a set of drains was installed on the superficial layer of the foundation (Ferreira et al., 2018).

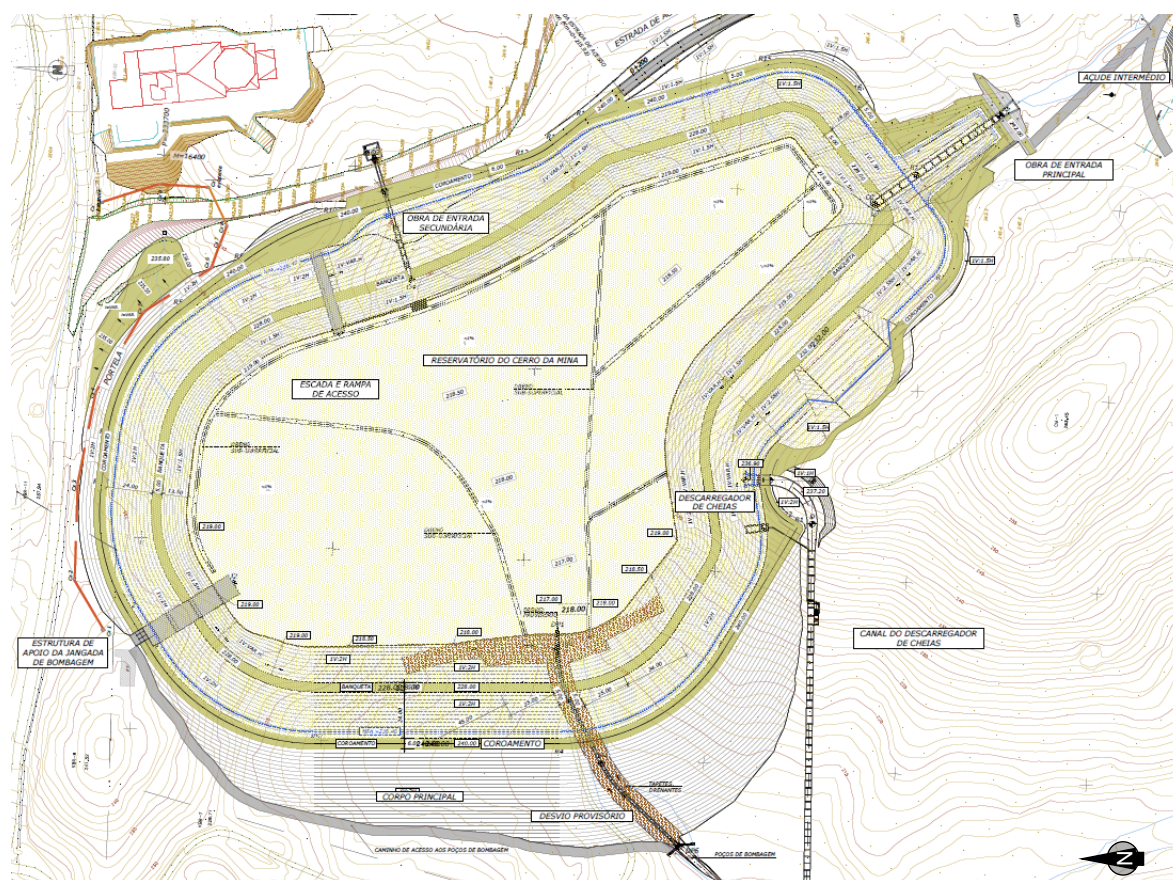


Figure 3.3 - Cerro da Mina Reservoir - General view of the structure (adapted from Cenor, 2010c).

The normal water level in the reservoir is 238,4 m, limited by a 5 m long uncontrolled spillway located on the left bank and an emergency outlet syphon. For a return period of 10.000 years, the discharge capacity of the spillway is 4,64 m³/s, whilst the syphon controls the discharge flow for water levels near the spillway crest with a maximum capacity of 0,47 m³/s. Due to the premiss of zero discharge, an intersection channel was constructed south of the structure to collect runoff water of an important part of the catchment area (Tavares et al., 2011).

3.1. Geological and geotechnical aspects and embankment zoning

Geological survey in the reservoir area found two main rock types from the Mértola Formation, typical of the region: greywackes and schists (siltstone and argillite). The greywackes are found in thick sub-horizontal layers, dip 5° to 10° NE, whilst the schists show thin stratification with 20° to 30° dip NE. In some areas, the excavations took place in well-defined zones of greywackes and schist. However, there were some sequences of less marked alternance of materials, in which schists and greywackes melded (Cenor, 2010e).

3.2. Rockfill characteristics

During the design phase, rock samples were collected from 3 investigation pits, 2 of greywackes and 1 of schist. An experimental fill was also executed, and 4 blocks were collected from it. Tests were conducted in type C material to determine physical and mechanical characteristics: unit weight, porosity, maximum water content, durability, resistance to degradation, resistance to crushing, uniaxial compression resistance and triaxial compression resistance. The results of all tests reproduced in this chapter were originally presented in the geological and geotechnical studies of the project (Cenor, 2010e).

To determine real density, apparent density, porosity, and maximum water content, 15 samples from the pits and 6 samples from 2 different blocs in the experimental fill were tested. Table 3.1 presents the results.

Table 3.1 - Real density, apparent density, porosity and maximum water content of the tested samples (after Cenor, 2010e).

| | Real density (kgm ⁻³) | Apparent density (kgm ⁻³) | Porosity (%) | Maximum water content (%) |
|--|--------------------------------------|--|-----------------|------------------------------|
| Greywacke / Investigation pit (10 samples) | | | | |
| Mean ± sd | 2712 ± 10.3 | 2581 ± 17.3 | 4.81 ± 0.83 | 1.86 ± 0.35 |
| Maximum | 2730 | 2600 | 4.0 | 2.5 |
| Minimum | 2700 | 2550 | 6.4 | 1.5 |
| Schist / Investigation pit (5 samples) | | | | |
| Mean ± sd | 2780 ± 7.1 | 2376 ± 60.3 | 14.56 ± 2.34 | 6.16 ± 1.15 |
| Maximum | 2790 | 2420 | 18.7 | 8.2 |
| Minimum | 2770 | 2270 | 13.0 | 5.4 |
| Greywacke / Experimental fill (6 samples) | | | | |
| Mean ± sd | 2702 ± 33 | 2588 ± 33 | 4.25 ± 0.71 | 1.65 ± 0.27 |
| Maximum | 2750 | 2620 | 5.4 | 1.4 |
| Minimum | 2670 | 2530 | 3.5 | 2.1 |

Slake durability tests were conducted in 6 samples from 3 different pits, of which 2 refer to greywackes and 1 to schists. Each sample was submitted to 7 cycles of 10 minutes at 20 rpm. The results are presented in Table 3.2 and indicates that the materials show high durability.

Table 3.2 - Slake durability tests results (after Cenor, 2010e).

| | Wet condition | | | Dry condition | | |
|-------------------------------|-----------------------|-----------------------|-----------------------|-----------------------|-----------------------|-----------------------|
| | 1 st cycle | 2 nd cycle | 7 th cycle | 1 st cycle | 2 nd cycle | 7 th cycle |
| Greywacke / Investigation pit | | | | | | |
| P1.1 | 3,9 | 5,3 | 10,0 | 1,3 | 1,8 | 2,9 |
| P1.2 | 2,6 | 3,3 | 6,0 | 0,9 | 1,3 | 2,5 |
| P2.1 | 2,4 | 3,7 | 8,6 | 0,6 | 1,0 | 2,3 |
| P2.2 | 1,6 | 2,1 | 4,0 | 0,8 | 1,2 | 2,1 |
| Mean ± sd | 2.6 ± 1.0 | 3,6 ± 1.3 | 7,2 ± 2.7 | 0,9 ± 0.3 | 1,3 ± 0.3 | 2,5 ± 0.3 |
| Schist / Investigation pit | | | | | | |
| P3.1 | 1,7 | 3,4 | 7,9 | 0,5 | 0,7 | 1,7 |
| P3.2 | 2,9 | 4,2 | 8,6 | 0,9 | 1,3 | 2,3 |
| Mean ± sd | 2,3 ± 0.8 | 3,8 ± 0.6 | 8,3 ± 0.5 | 0,7 ± 0.3 | 1,0 ± 0.4 | 2,0 ± 0.4 |

Three samples from the investigation pits and one collected in the experimental fill were used to determine the resistance to degradation by abrasion and impact in the Los Angeles Machine. The results shown in Table 3.3 suggest the materials have high resistance to abrasion.

Table 3.3 - Los Angeles abrasion test results (after Cenor, 2010e).

| Lithology / Origin | Sample | Grading | Loss (%) |
|-------------------------------|--------|---------|----------|
| Greywacke / Investigation pit | P1.1 | F | 35 |
| | P2.1 | G | 43 |
| Schist / Investigation pit | P3.1 | F | 44 |
| Greywacke / Experimental fill | 9/13 | F | 27 |

Crushing tests were conducted in samples of greywackes and schists according to the methodology proposed by Wilson and Marsal (1979). The test consists in determining the load necessary to break particles of 3 different diameters, establishing an empirical relation that follows the Equation (4):

$$Pa = \eta D^\lambda \quad (4)$$

where Pa is the resistance to crushing, D is the average diameter, and η and λ are empirical coefficients. It is also common to determine PA₅₀, the resistance to crushing for the theoretical

diameter of 50mm. The results are presented in Table 3.4 and reveals that the materials have an adequate resistance to crushing.

Table 3.4 - Results of the crushing resistance test (after Cenor, 2010e).

| Test conditions | | η (kgf.cm ³) | λ | Pa ₅₀ (kgf) |
|---|---------------|-------------------------------|---------------|------------------------|
| Greywacke / Investigation pit (4 samples) | | | | |
| Air dried | Mean \pm sd | 64.0 \pm 3.4 | 1.8 \pm 0.2 | 1219.3 \pm 377.7 |
| | Maximum | 67.0 | 2.0 | 1582 |
| | Minimum | 60.6 | 1.5 | 692 |
| Saturated | Mean \pm sd | 41.2 \pm 17 | 1.8 \pm 0.3 | 690.0 \pm 217.5 |
| | Maximum | 65.4 | 2.0 | 986 |
| | Minimum | 26 | 1.3 | 505 |
| Schist / Investigation pit (2 samples) | | | | |
| Air dried | Mean \pm sd | 51.8 \pm 20.4 | 1.8 \pm 0.2 | 911.0 \pm 17.0 |
| | Maximum | 66.2 | 2.0 | 923 |
| | Minimum | 37.4 | 1.6 | 899 |
| Saturated | Mean \pm sd | 27.2 \pm 10.5 | 1.5 \pm 0.5 | 316.0 \pm 123.0 |
| | Maximum | 34.6 | 1.9 | 403.0 |
| | Minimum | 19.7 | 1.2 | 229.0 |
| Greywacke / Experimental fill (1 sample) | | | | |
| Air dried | | 38.5 | 2.0 | 1033.0 |
| Saturated | | 18.4 | 2.1 | 506.0 |

Granulometric analysis were conducted in 30 samples collected in type C material during the construction of the rockfill. The results are presented in Figure 3.5, in which it is possible to notice that most curves are in the zone between the specified limits.

In order to determine the uniaxial compressive strength of the rocks, 10 samples of greywacke and 5 samples of schist were tested. The dimensions of the specimens were approximately 50 x 50 x 125 mm³. The results are shown in Table 3.5.

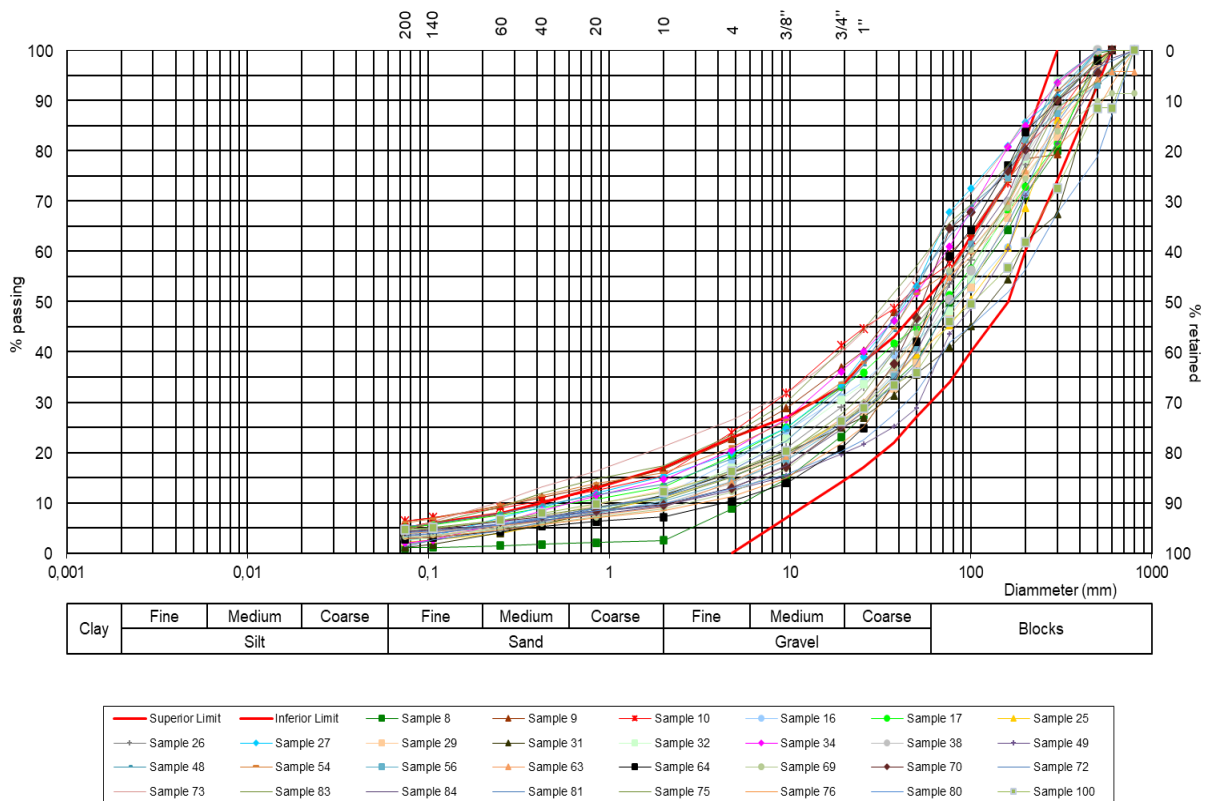


Figure 3.5 - Granulometric analysis of type C material sampled during construction (after Cenor, 2010e).

Table 3.5 - Results of uniaxial compressive strength tests (after Cenor, 2010e).

| | Uniaxial compressive strength (MPa) | | |
|-----------|--|---|---|
| | Greywacke / Investigation pit (10 samples) | Schist / Investigation pit (3 samples) ¹ | Schist / Investigation pit (2 samples) ² |
| Mean ± sd | 40.0 ± 4.4 | 11.0 ± 1.7 | 6.1 ± 2.6 |
| Maximum | 46.9 | 13.0 | 7.9 |
| Minimum | 31.6 | 9.8 | 4.2 |

¹ load applied parallel to the schistosity plane; ² load applied normal to the schistosity plane

To determine shear resistance of the rockfill, drained triaxial tests on large cells were conducted in samples using material from investigation pit P1. Specimens with 308 mm of diameter and 720 mm of height were used in the tests. In spite of the equipment’s large dimensions, particles larger than 50 mm could not be utilized in the specimens. To prepare the samples, a homothetic distribution of the mean curve was employed, and particles larger than 50 mm were

proportionally replaced by elements between 3/4” and 2”. Figure 3.6 shows the curves representing the superior and inferior limits defined for the material, the mean distribution and the one tested.

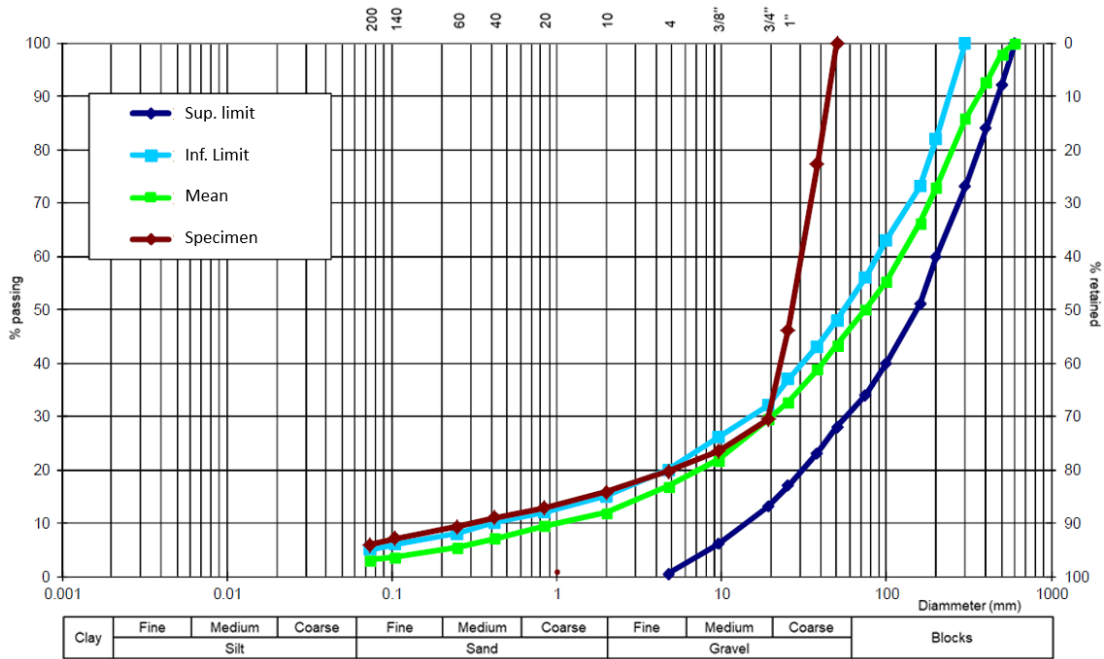


Figure 3.6 - Granulometric distribution: superior and inferior limits, mean distribution and tested specimen (adapted from Cenor, 2010e).

The compaction of each specimen was achieved by vibrating 11 layers of equal mass for 12 minutes each. Table 3.6 presents dry unit weight, moisture contents before and after testing and the results of vertical permeability tests executed before saturation phase. The evolution of grain size distribution was assessed by new granulometric analysis conducted after testing, as represented in Figure 3.7.

Table 3.6 - Specimens characteristics (after Cenor, 2010e).

| Confining stress (kPa) | Initial dry unit weight (kN/m ³) | Initial moisture content (%) | Final moisture content (%) | Permeability (m/s) |
|------------------------|--|------------------------------|----------------------------|------------------------|
| 150 | 18,80 | 3,5 | 8,4 | 9,0 x 10 ⁻⁶ |
| 300 | 18,73 | 3,5 | 7,1 | 9,5 x 10 ⁻⁶ |
| 600 | 18,86 | 3,5 | 7,3 | 8,7 x 10 ⁻⁶ |

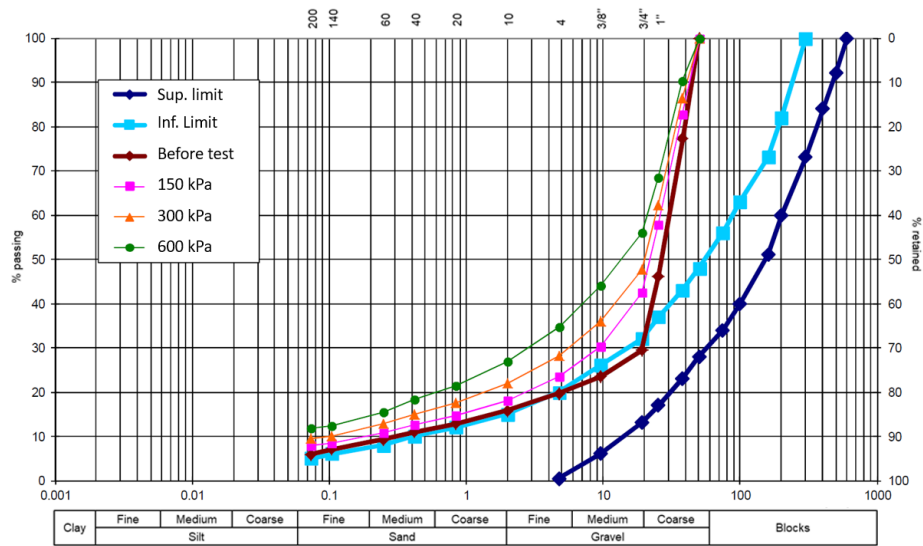


Figure 3.7 - Grain size distribution: Superior and inferior limits and specimens before and after triaxial tests (adapted from Cenor, 2010e).

It is possible to notice some evolution in the granulometric characteristics of the specimens after the test, showing more importance as the confining stress increases. This behaviour is related to particle breakage and contact crushing, and might be considered expected. The results of the triaxial tests in terms of mean stress versus axial deformation and axial deformation versus volumetric deformation are depicted in Figure 3.8 and Figure 3.9, respectively. It is possible to notice the absence of peak in the stress-strain curves, showing that the material tends to have a ductile response.

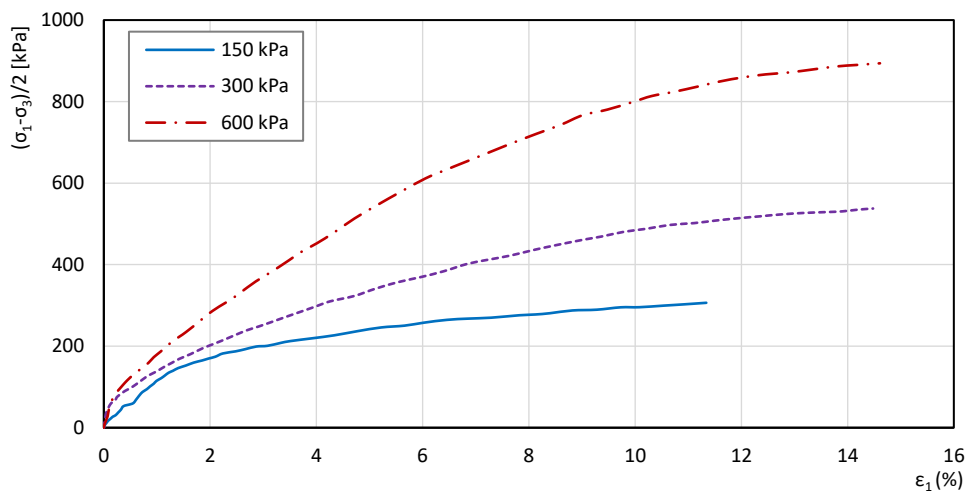


Figure 3.8 - Mean stress vs axial deformation of the 3 specimens tested in the large triaxial cell (after Cenor, 2010e).

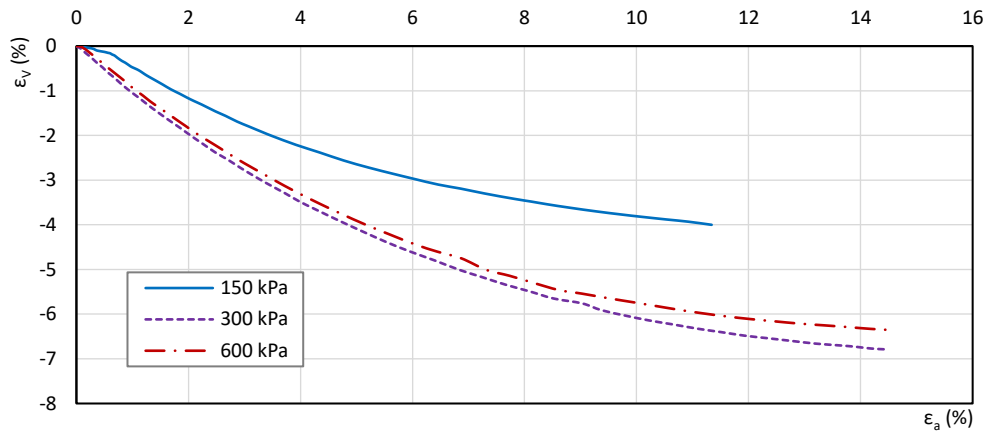


Figure 3.9 - Axial vs volumetric deformation of the 3 specimens tested in the large triaxial cell (after Cenor, 2010e).

The results of the triaxial tests are shown in terms of stress trajectories in the $s' \times t$ space, as presented in Figure 3.10. The internal friction angle of the sample, based on a linear regression of the maximum deviatoric stress reached by the specimens, was estimated in 37.7° . Nevertheless, a linear failure envelope may not be the most representative for the material, since in rockfill frequently the friction angle varies according to stress state (Tapias et al., 2015), showing an inverse relation with the confining stress, and for this sample it was not different. The values of the confining stress, peak principal stresses, slope of the critical state line M and internal friction angle for each specimen are presented in Table 3.7. A correlation between internal friction angle and confining stress, represented by the logarithm of the minor principal stress divided by atmospheric pressure, is represented in Figure 3.11.

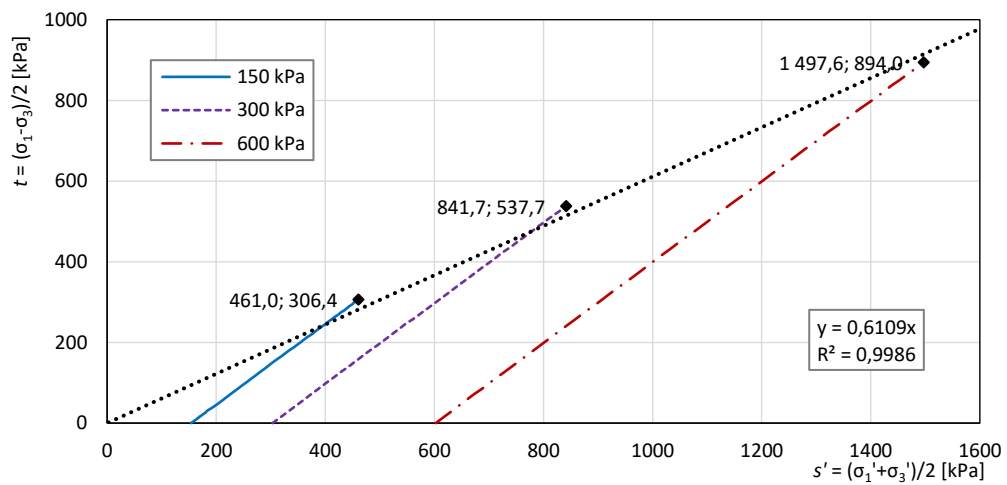


Figure 3.10 - Stress trajectory of the 3 specimens tested in the large triaxial cell (after Cenor, 2010e).

Table 3.7 - Internal friction angle as a function of confining stress (after Cenor, 2010e).

| σ'_{30} (kPa) | σ'_{1f} (kPa) | σ'_{3f} (kPa) | M | ϕ' (°) |
|-------------------------|-------------------------|-------------------------|------|----------------|
| 150 | 767,4 | 154,6 | 1,71 | 41,7 |
| 300 | 1379,4 | 304,0 | 1,62 | 39,7 |
| 600 | 2391,6 | 603,6 | 1,49 | 36,7 |

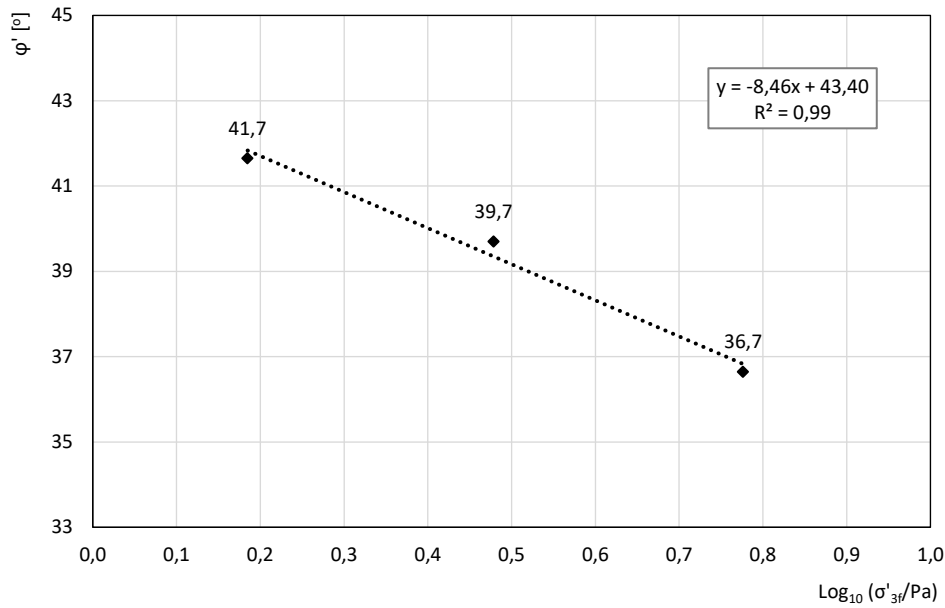


Figure 3.11 - Variation of internal friction angle concerning confining stress (after Cenor, 2010e).

From the regression presented in Figure 3.11, it is possible to determine the correlation between expected internal friction angle and confining stress (Equation 5). Based on that, a non-linear failure envelope was created, using Equation 6. As shown in Figure 3.12, this curve fits more appropriately the failure points obtained in the triaxial tests.

$$\phi' = 43.4 - 8.46 * \log \frac{\sigma'_{3f}}{\text{Pa}} \quad (5)$$

$$\sigma'_{1f} = -\sigma'_{3f} * \frac{\sin(\phi'+1)}{\sin(\phi'-1)} \quad (6)$$

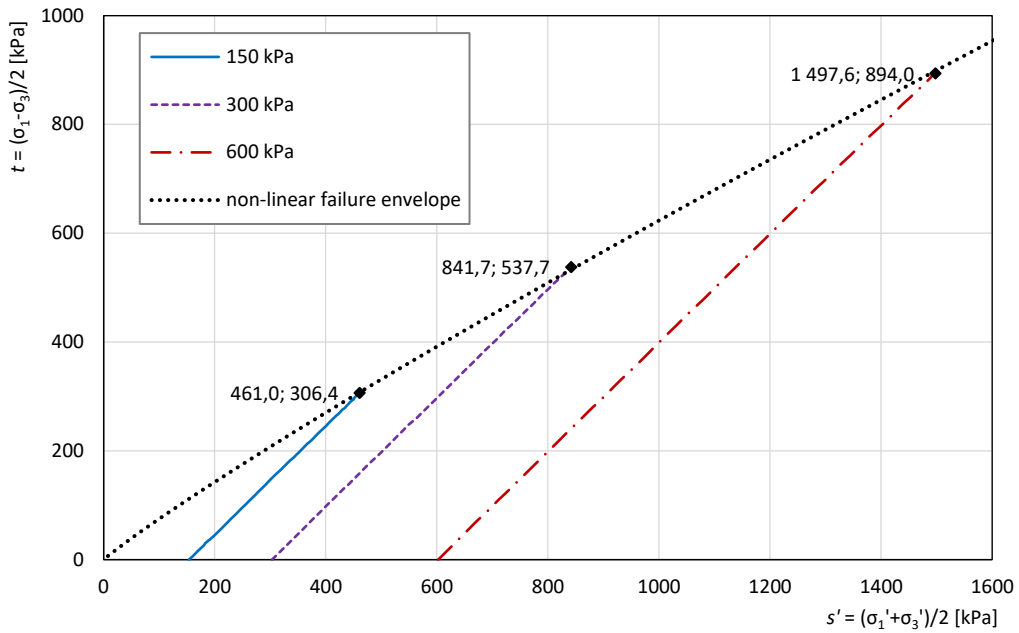


Figure 3.12 - Non-linear failure envelope for the rockfill.

The triaxial tests conducted were also used to determine rockfill compressibility. Young modulus was determined for an axial deformation of 0,1%, as depicted in Figure 3.13 for the three specimens tested (Tavares et al., 2015).

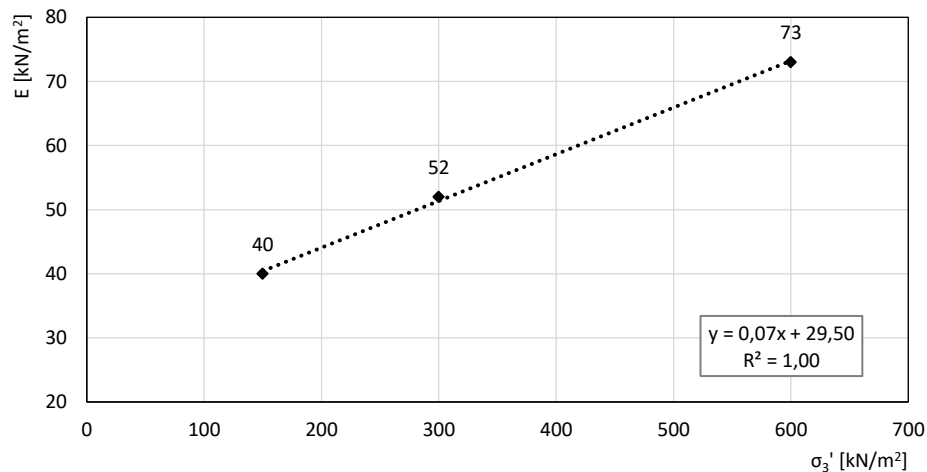


Figure 3.13 - Young modulus of the specimens for 0,1% axial deformation (Tavares et al., 2015).

According to the rockfill classification methodology proposed by Wilson and Marsal (1979), this material may be rated as soft well-graded to semi-hard well-graded rockfill. B_g values were

between 3,4% and 7,7%, and the relation between principal stresses at failure presented values between 1,9 and 3,7 (Tavares et al., 2015).

3.3. Instrumentation plan

The instrumentation plan was conceived according to the Portuguese dam safety regulation and specificities of the reservoir. The instruments existent in the facility are as follows (Ferreira et al., 2018):

- 25 surface settlement markers in the crest (17 in the main embankment, 8 in the saddle embankment), installed 25 meters distant from each other.
- 3 inclinometers associated to vertical magnet extensometers, with measurement sections each 3 meters, installed during the construction phase.
- 23 hydraulic piezometers: 5 instruments upstream of the reservoir; 2 devices in the foundation, beneath the rockfill; 2 piezometers in the interface rockfill / foundation; and 14 instruments downstream of the reservoir, in which also water samples for chemical analysis are collect.
- 3 pumping wells installed in the toe of the downstream slope, measuring seepage in the sub-superficial drainage system of the embankment.
- 2 staff gauges indicating the water level in the reservoir, supported by topographic measurements.
- 2 meteorological station, already existent in the mining compound.

Figure 3.14 and Figure 3.15 present, respectively, the highest cross section, PO3, with its monitoring devices, and a map with the location of the instruments installed in the embankment.

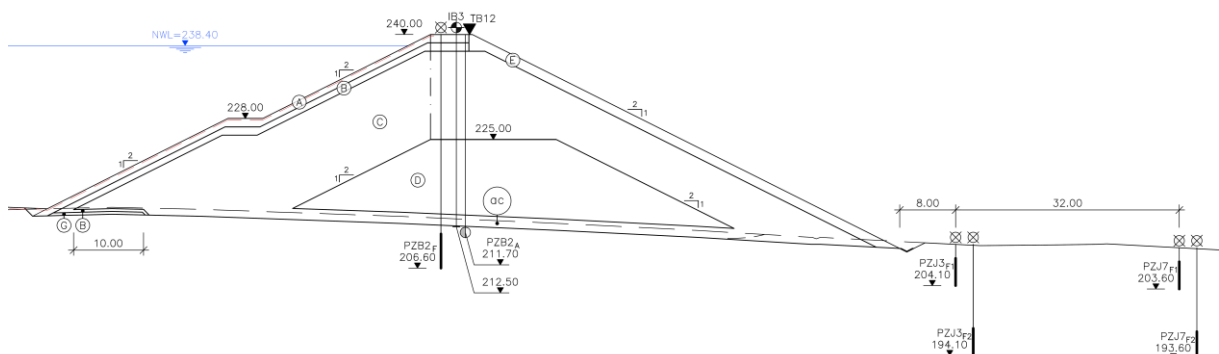


Figure 3.14 - Cross section PO3 (adapted from Cenor, 2010a).

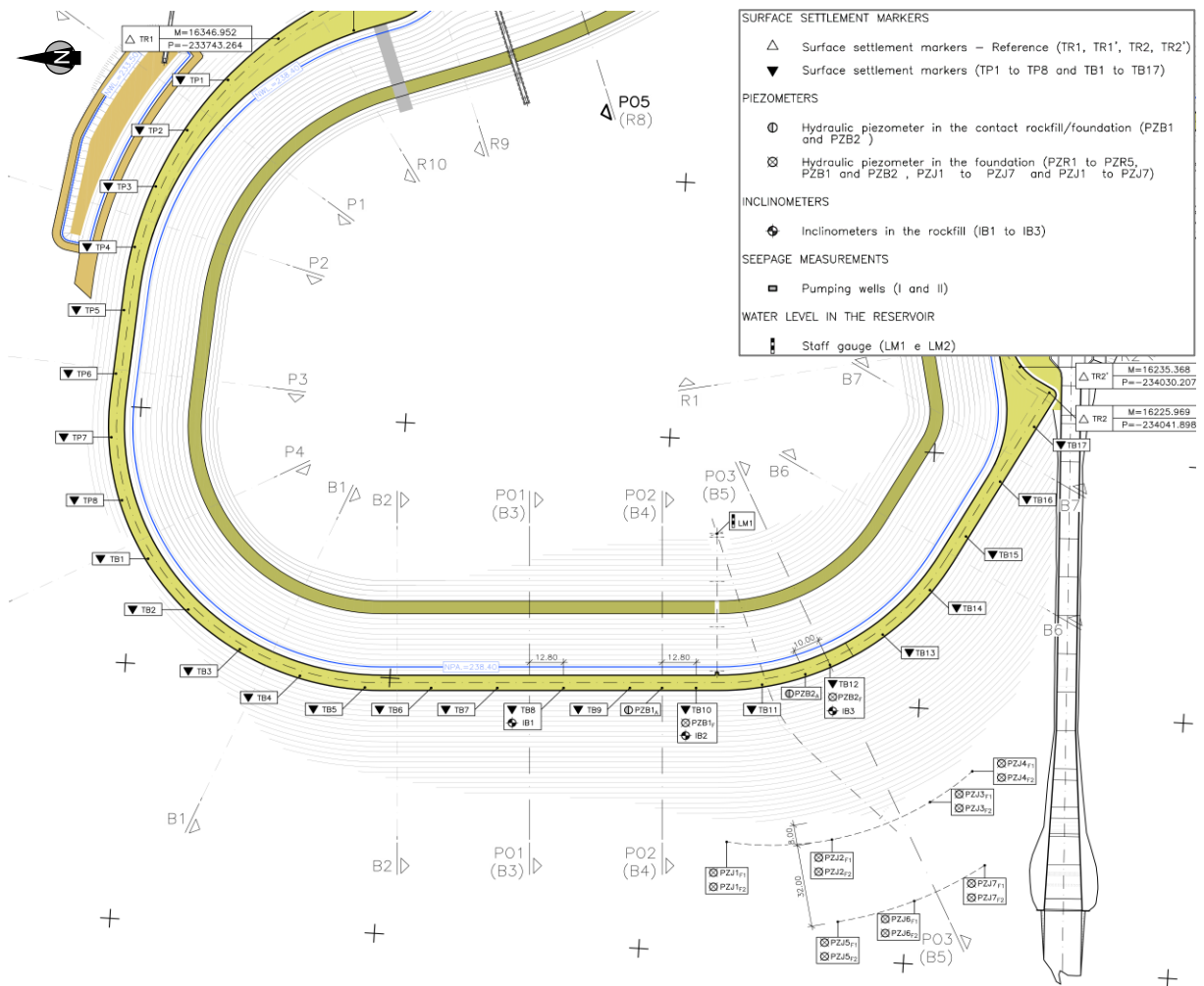


Figure 3.15 - Location of the instruments installed in the embankment (adapted from Cenor, 2010b).

The frequency of the observations was determined considering the recommendations of the Portuguese Standard for Observation and Inspection of Dams (Norma de Observação e Inspeção de Barragens – NOIB). The only exception is the flow measurements, which has a higher frequency than preconized by NOIB, due to its relevance to assess of the well function of the impervious membrane. Table 3.8 presents the frequency of observations (Cenor, 2011).

Table 3.8 - Frequency of observations

| Observation | Phase of the construction | | | | |
|--------------------------|---------------------------|---|------------------------------------|----------------|----------------|
| | Construction | First filling | Exploration | | |
| | | | First 5 years | After 5 years | |
| Superficial displacement | - | Beginning, platform and completion | Annually | Every 2 years | |
| Internal displacement | Every 15 days | Beginning, platform and completion | Every 6 months | Every 6 months | |
| Discharge | - | Weekly | Weekly | Weekly | |
| Porewater pressure | Weekly | Beginning, platform and completion | Every 3 months | Every 3 months | |
| Visual inspections | Routine | Weekly | Beginning, platform and completion | Every 3 months | Every 3 months |
| | Speciality | Half of the construction and after completion | Beginning, platform and completion | Annually | Every 2 years |
| | Exceptional | After event | After event | After event | After event |
| Water level | - | Daily | Daily | Daily | |

4. Assessment of the monitoring results

As mentioned in the introductory chapter, instruments installed in the rockfill embankment of Cerro da Mina Reservoir recorded some unexpected deformations in different moments. Under constant load, the largest settlements are normally anticipated at the beginning of the operation of the dam, and the rates in which strains occur are expected to reduce over time. In this case, however, vertical extensometers installed in the rockfill recorded a few peaks of movements years after the end of construction and first filling. The moments of increase in the settlement rates coincided with periods of large pluviosity when, naturally, the water level in the reservoir and the moisture in the rockfill rise. These two factors were indicated as possible causes of this unexpected deformations, and their influence have to be investigated in order to reach a more conclusive explanation for the behaviour.

The measurements recorded by the instruments installed in the highest section of embankment, PO3 (Figure 3.14 and Figure 3.15), were chosen to be the object of this analysis. Inclinator IP3 is located on the crest of the embankment in that section, alongside with nine vertical extensometers distributed in the rockfill, consisting of magnet rings placed externally to the inclinometer casing tube. Figure 4.1 depicts the location of the rings and their initial elevations.

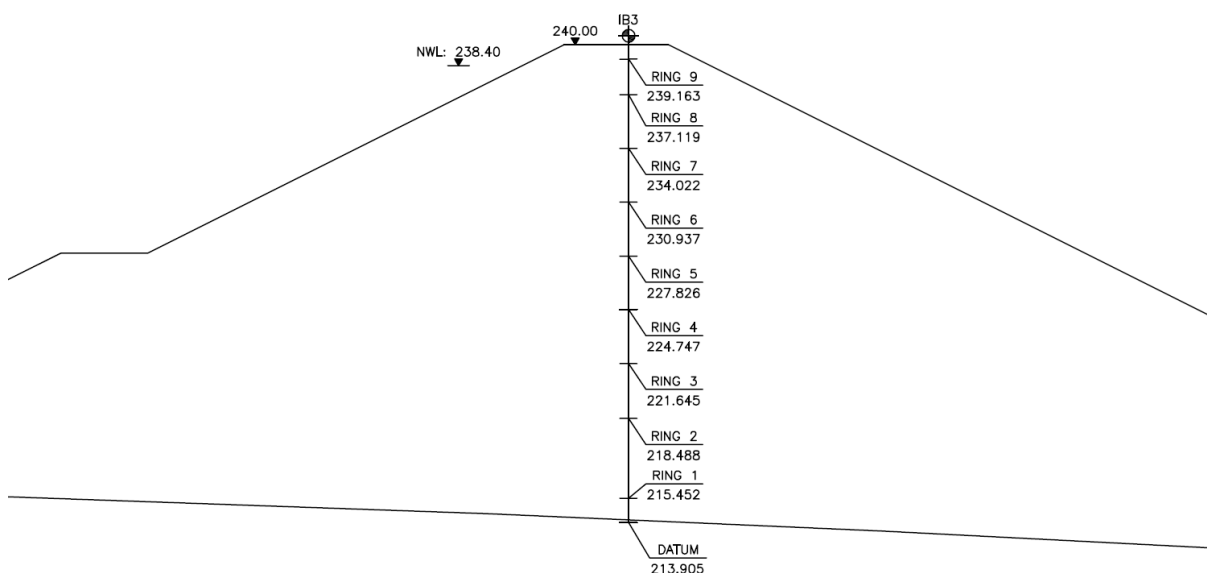


Figure 4.1 - Extensometers installed in section PO3 (adapted from Cenor, 2010a).

4.1. Vertical displacements in the rockfill

The analysis of the vertical displacements recorded in the rockfill comprises the period between December of 2013 (the first time all nine rings were read) and September 2020. In this period, no relevant seismic activity was recorded, nor any leakage in the HDPE membrane. Figure 4.2 presents the vertical displacements measured in the nine extensometers installed in section PO3.

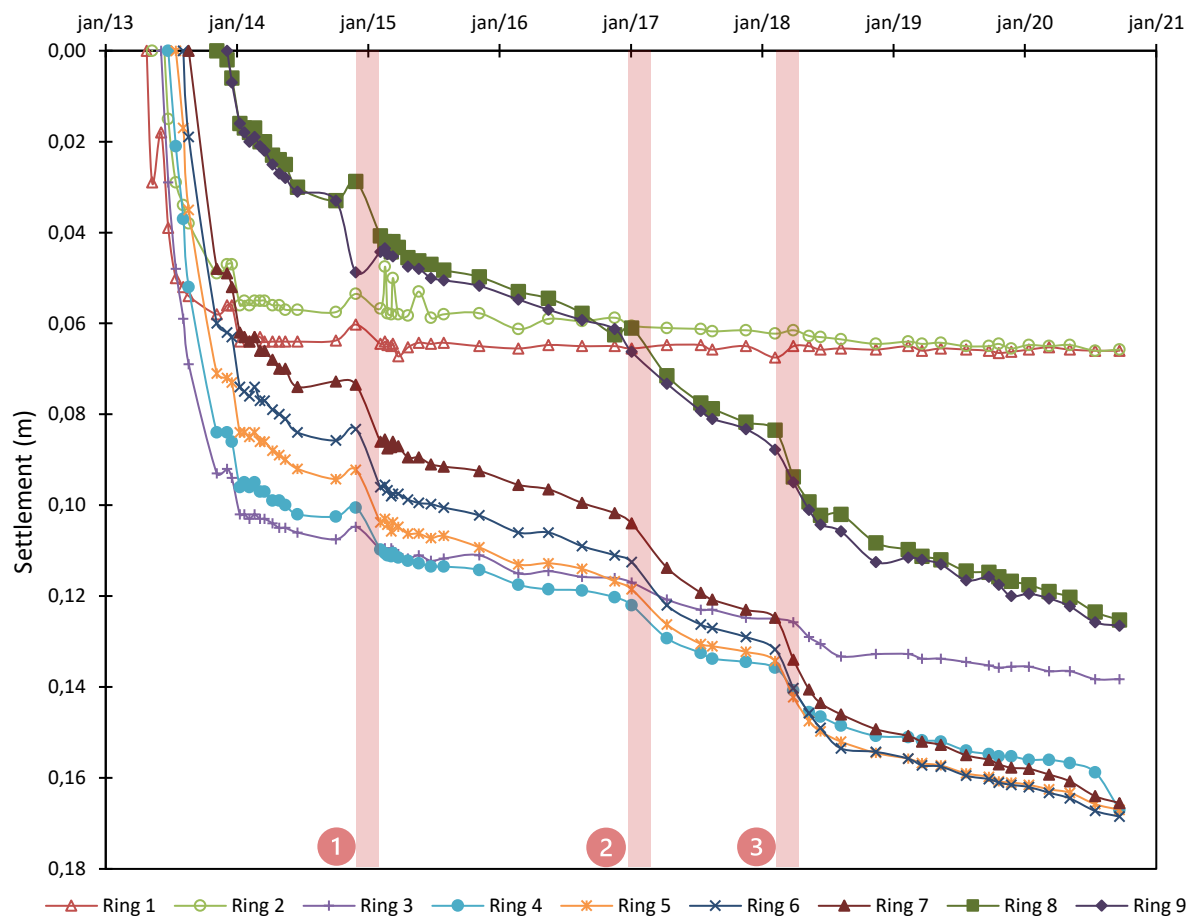


Figure 4.2 - Settlement of the extensometers installed at IB3.

The form of the vertical displacement curves in the first year (between the end of 2013 and November of 2014) was similar to the expected, with the general shape of the curves resembling a logarithmic relation in time, steeper in the beginning, reducing inclination after the first few months and showing a tendency to future stabilization. In the first reading of 2015, however, the behaviour registered in most of the extensometers changed (exceptions are rings 1 and 2, which kept their tendencies almost constant), with a new increase in the settlement rate. After that moment, the form of the curves started again to indicate that the vertical displacements

would probably return to the expected behaviour, i.e., a tendency to show reduction in the rate of movements. This performance was kept until the first months of 2017, when, again, the settlement rate showed a sudden increase. The entire behaviour then repeated itself. This happened again once more, with a new abrupt settlement occurring between February and March 2018, this one even more prominent than the before. These moments are highlighted in Figure 4.2 and numbered 1 to 3. After that last increase, there has not been any unexpected deformation, and the trend registered in the extensometers has been as expected. Figure 4.3 presents a graphical representation of vertical displacement versus elevation of the extensometer, in which the referred moments of behaviour change can be also noticed by the larger spaces between adjacent curves, since the measurements are fairly regular. Nevertheless, the overall aspect of the graph resembles what is expected for a regular embankment, showing no clear sign of unusual behaviour.

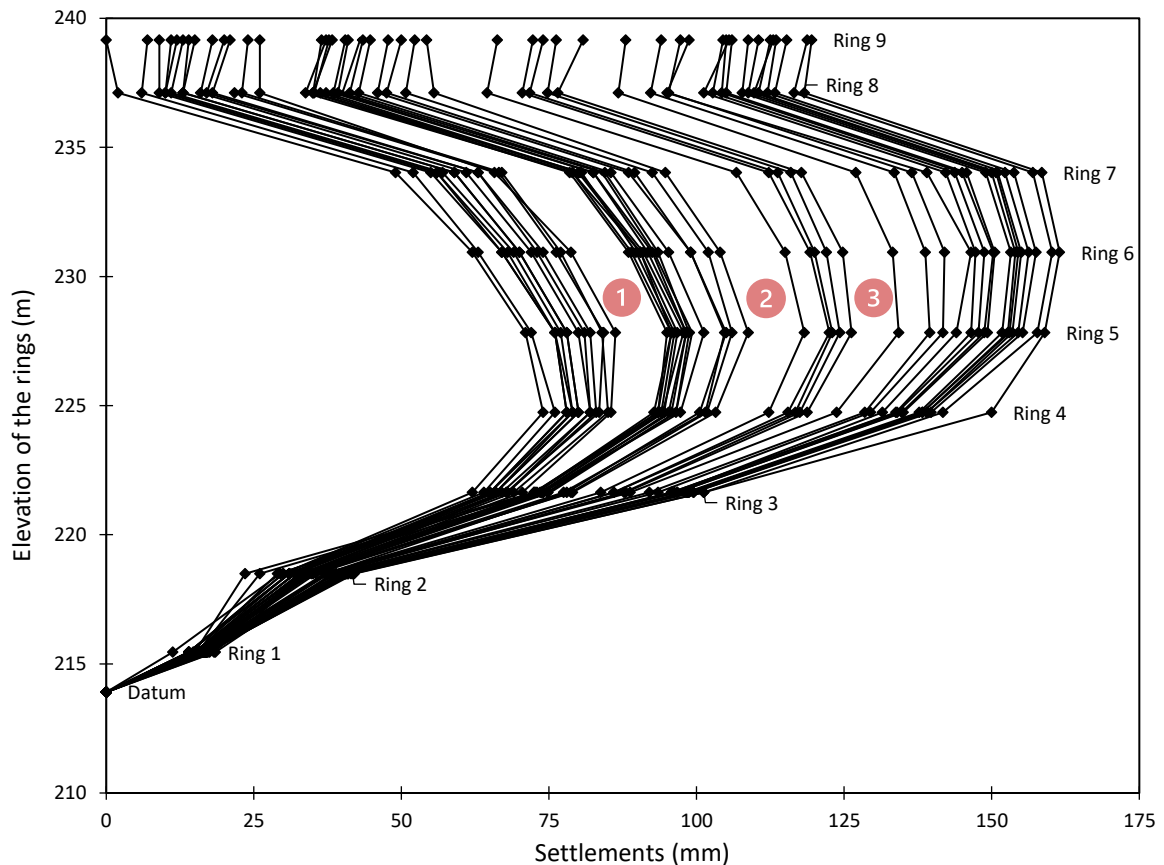


Figure 4.3 - Relation between elevation of the extensometer and vertical displacement.

It must be referred that Figure 4.2 shows a reduced swell (between 1 and 4 mm) in 8 of the 9 extensometers (exception is Ring 9) in the last months of 2014. That unusual record can be associated to a problem in the measurements, since there is no apparent reason for that

behaviour. It is also relevant to mention that Rings 1 and 2 showed no significant change in their behaviour over time, and therefore are not analysed with the other rings. Considerations about these particular extensometers are made at the end of this section.

As mentioned, the alterations of trend recorded in the settlement curves in 3 moments (between November 2014 and January 2015, between January and April 2017 and between February and May 2018) were not expected. Those periods were associated to increases in the water level in the reservoir and intense rainfall, which rose questions about the influences of each of those factors in the deformation mechanisms in the embankment. Figure 4.4 and Figure 4.5 present the records of water level in the reservoir and pluviosity, with the three mentioned periods highlighted.

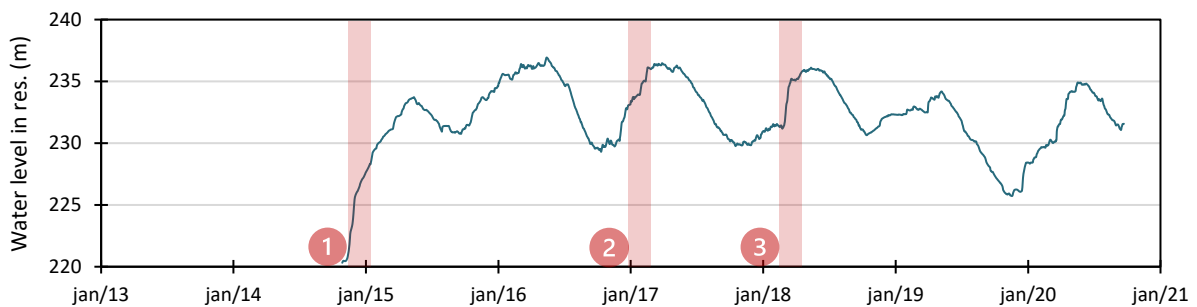


Figure 4.4 - Oscillation of the water level in the reservoir.

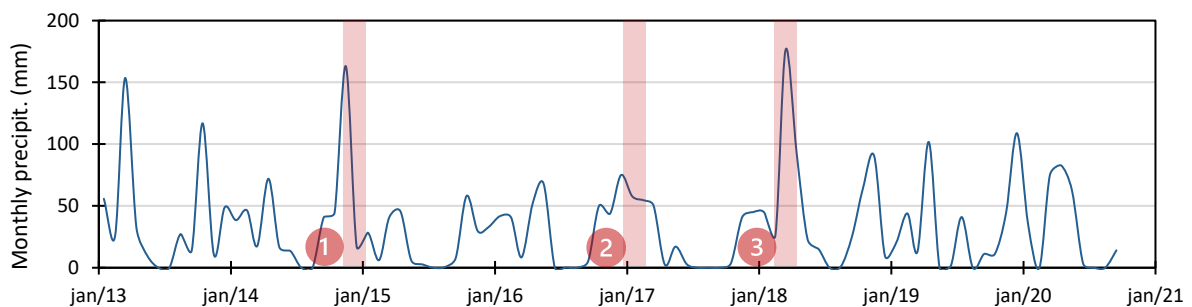


Figure 4.5 - Monthly precipitation in the reservoir area.

Figure 4.4 shows that the first filling of the reservoir started in the last months of 2014. The water level in the pond presents a fairly regular oscillation, with increases associated to intense rainfall periods and decreases associated to dry periods. The water table never passed (until September 2020) elevation 237 m, and fluctuations were always smaller than 10 meters. In Figure 4.5, the moments in which the unexpected settlement rates were recorded match the periods of most intense pluviosity. Although there is no clear peak in the monthly precipitation

in early 2017, like it happens in the other two moments (November 2014 and March 2018), that period corresponded to 5 consecutive rainy months, which provided a substantial accumulated pluviosity, even larger than the recorded in late 2014.

Since the reservoir is considered as impervious, there is no percolation in the rockfill directly associated to the pond, and fluctuations in the water level only modifies the load (and consequently the stresses) in the embankment. Pluviosity, on the other hand, has direct impact on the water content in rockfill, changing humidity in the large voids between elements and suction in the rock pores, thus altering the stress state in the rockfill as well. The possible contributions of each of these factors to the deformations recorded in the embankment were analysed. To assess how the variation of the water load affects the stress state in section PO3, a numerical model created during the design phase was used to calculate the expected vertical stress in the inclinometer IB3 section for two conditions: before filling (totally empty pond) and normal water level (elevation 238.40 m). The tension points chosen to evaluate vertical stress were located halfway between adjacent magnet rings. Table 4.1 presents the results, where it is possible to notice small changes in the vertical effective stress in those points.

Table 4.1 - Effective vertical stress calculated in section PO3.

| | Effective vertical stress (kPa) | | |
|-----------------|---------------------------------|--------------------|-----------|
| | Before filling | Normal water level | Variation |
| Datum - Ring 1 | 525.4 | 539.7 | +2.7% |
| Ring 1 - Ring 2 | 486.2 | 498.5 | +2.5% |
| Ring 2 - Ring 3 | 424.6 | 433.9 | +2.2% |
| Ring 3 - Ring 4 | 361.0 | 368.3 | +2.0% |
| Ring 4 - Ring 5 | 303.1 | 308.2 | +1.7% |
| Ring 5 - Ring 6 | 240.3 | 243.0 | +1.1% |
| Ring 6 - Ring 7 | 177.5 | 178.9 | +0.8% |
| Ring 7 - Ring 8 | 122.2 | 122.7 | +0.4% |
| Ring 8 - Ring 9 | 61.8 | 62.0 | +0.3% |

The reduced oscillation in the estimated vertical stress indicates that the load due to the water in the pond does not have a significant influence in the stress state in the rockfill in the analysed section. Since RCM is considered an impervious reservoir, the difference between empty pond and normal water level lays on the load applied on the upstream slope of the embankment, and although it causes a small rotation in the principal stress direction at section PO3, the values of vertical stress does not increase significantly. It is relevant to draw attention to the fact that the variation of vertical stress presented on Table 4.1 refers to the maximum oscillation of water table possible (approximately 23 m of difference in section PO3), whereas the fluctuation of

the water level after the first filling was, in reality, less than 8 m. This means that the changes that actually occurred in the vertical stress in that section were expected to be smaller than the calculated.

Besides the small effect on the vertical stress in the extensometers, three other relevant aspects support the conclusion that variation of water load is probably not the main mechanism involved in the unexpected settlements. First, the moment in which the water level reached its maximum value (May of 2016) does not correspond to any of the 3 peaks verified in the settlement rate, as Figure 4.6 presents. Second, the extensometers have not recorded any swell associated to the partial drawdowns of the reservoir. If those increases in vertical stress were the main cause for additional compression of the rockfill, decreases should produce some level of extension (or at least significant reduction in the settlement rate), which did not happen. The third point relates to the fact that after the maximum load was reached for the first time, the materials would be subject to unload-reload cycles, in which the stiffness of the rockfill would be substantially higher. Therefore, the deformations associated to the fluctuation in the water table following that moment should be much smaller than the associated to the first filling, differently from what really occurred.

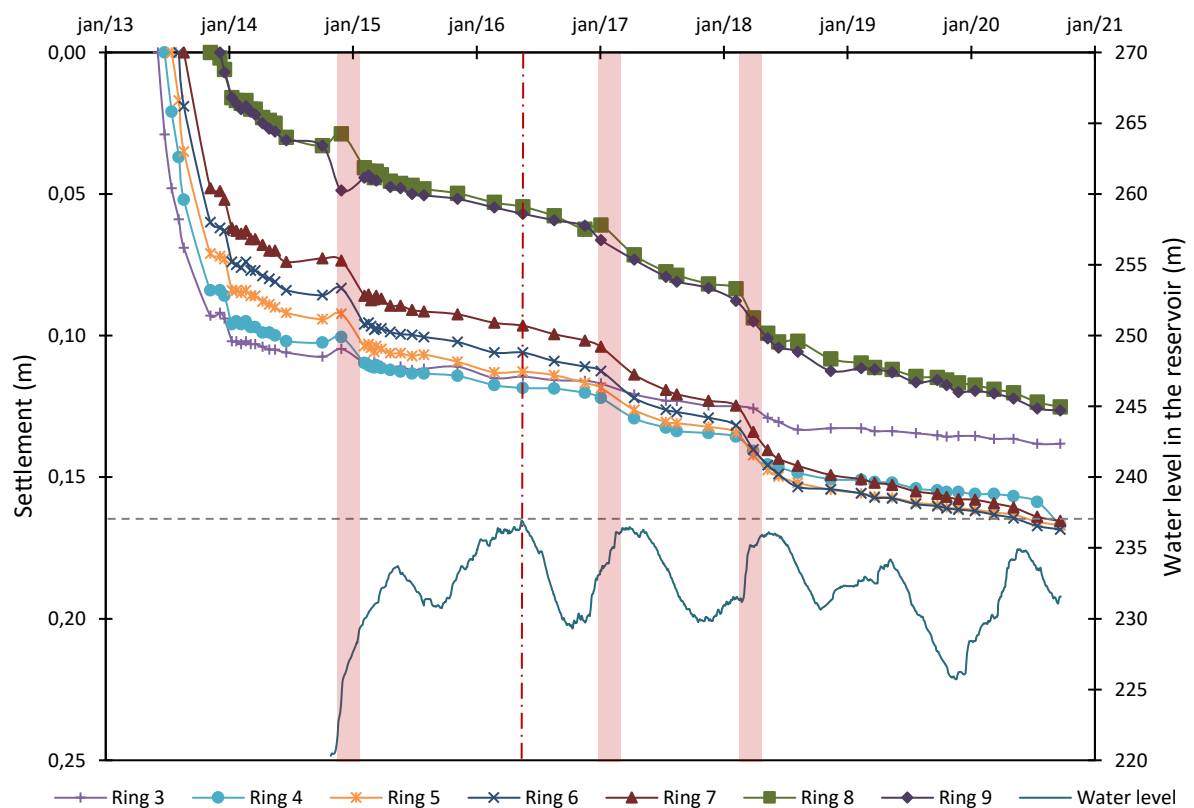


Figure 4.6 - Vertical displacements of the extensometers and water level in the reservoir.

Since the fluctuations of the water level in the reservoir cannot be indicated as the main cause of the abrupt settlements in the rockfill, pluviosity emerges as the probable origin of the unexpected vertical displacements recorded in the embankment, more specifically through the phenomenon of wet-induced collapse. In impervious faced dams, such as RCM, this mechanism is commonly associated to periods of very intense pluviosity, particularly when a new historical maximum is recorded, since after each collapse only a larger occurrence is expected to trigger new abrupt settlement. The theory supporting this proposition is presented in Chapter 2 of this dissertation. To assess if this could be the mechanism taking place in RCM, the values of accumulated precipitation in periods of consecutive rainy months were analysed, starting in December of 2013. Table 4.2 presents the measurements.

Table 4.2 - Accumulated precipitation in RCM area between December 2013 and September 2020.

| Period | Accumulated precipitation | Historical maximum | Collapse |
|--------------------------------|---------------------------|--------------------|----------|
| December 2013 – April 2014 | 223 mm | - | - |
| September 2014 – November 2014 | 249 mm | Yes | Yes (1) |
| March 2015 – April 2015 | 86 mm | No | No |
| October 2015 – February 2016 | 203 mm | No | No |
| April 2016 – May 2016 | 120 mm | No | No |
| October 2016 – May 2017 | 332 mm | Yes | Yes (2) |
| November 2017 – May 2018 | 448 mm | Yes | Yes (3) |
| September 2018 – November 2018 | 180 mm | No | No |
| April 2019 | 102 mm | No | No |
| November 2019 – January 2020 | 188 mm | No | No |
| March 2020 – May 2020 | 220 mm | No | No |

From Table 4.2 it is possible to verify that all three moments of collapse correspond to the highest record of accumulated precipitation until that moment, and no historical maximum occurred without an abrupt settlement. Figure 4.7 illustrates this statement, in which it is possible to see that the three periods of most intense pluviosity (delimited by dashed lines) were overlapped with the three moments when collapse occurred. This bijective relation strengthens the perception that wet-induced collapse is the mechanism responsible for the sudden increases in the rates of vertical displacement recorded in the embankment.

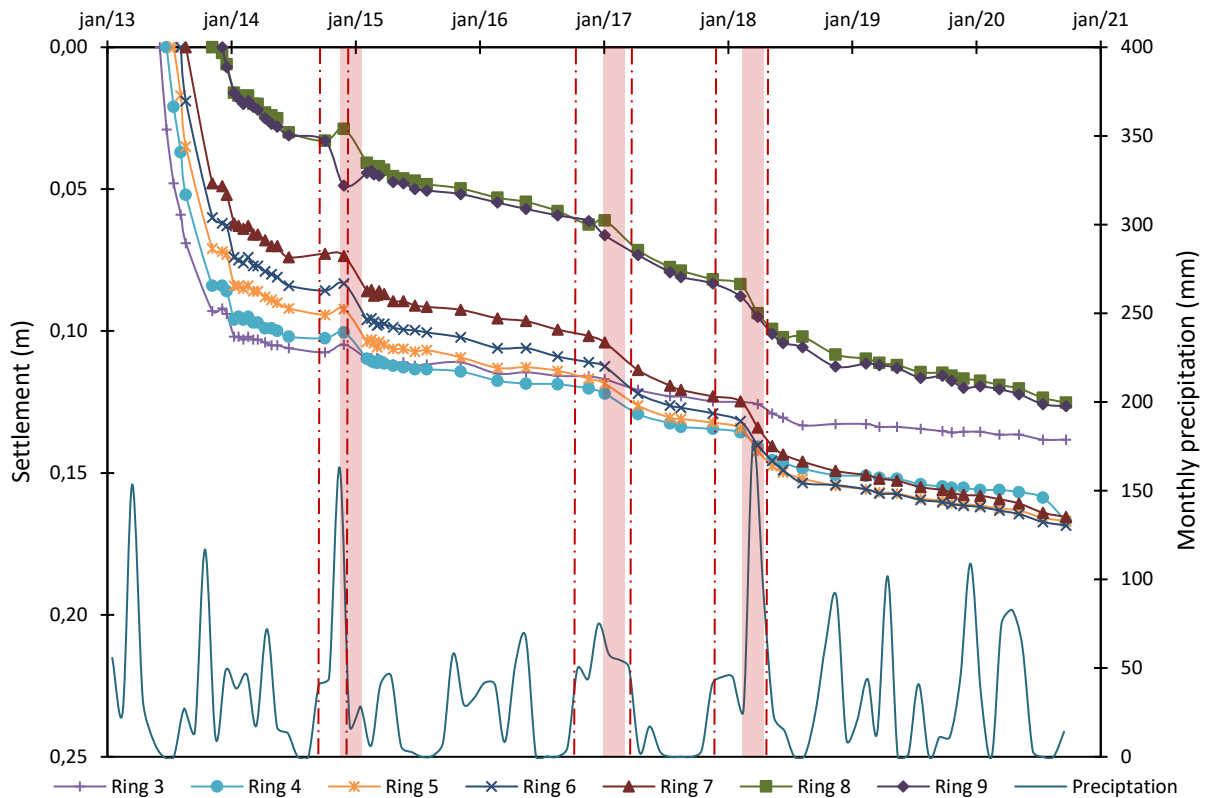


Figure 4.7 - Vertical displacement of the extensometers and monthly precipitation.

It is relevant to refer that, besides the three analysed moments of abrupt vertical displacement, the period covering December of 2013 to April of 2014 also exhibited a very substantial settlement rate, along with significant pluviosity. Nevertheless, since this occurred only few months after the construction was completed, deformations are naturally expected to be more intense at that point, and it is not possible to determine if wetting collapse happened, and how much it would have added to the overall strains already occurring then. For that reason, this particular period was not considered in the analysis.

Figure 4.8 presents the relation between the vertical displacement due to collapse and the increase in the historical maximum of precipitation. It is not possible to define a clear trend that relates to all the extensometers regarding whether the increase in the accumulated rainfall influences the amount of vertical displacement. However, it may be noticed that, in all rings, the last collapse recorded was the largest of the three.

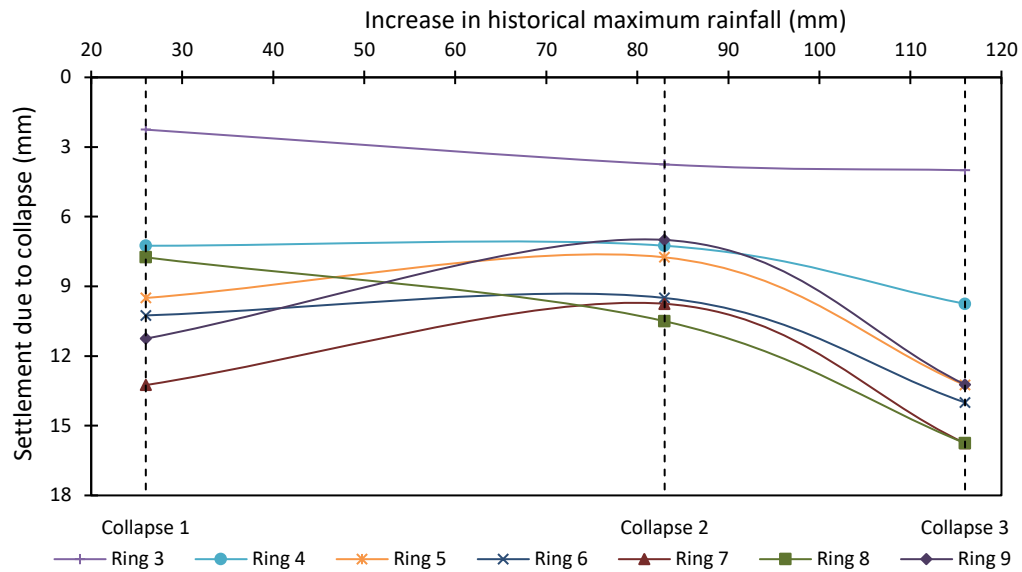


Figure 4.8 - Settlement due to collapse and increase in historical maximum accumulated rainfall in the period of analysis.

Although there are really strong indications that the settlements recorded are clearly related to pluviosity, wet-induced collapse depends directly on the suction existent in the voids of the rockfill elements, which could not be assessed in this case. However, water pressure in the rockfill is expected to be very dependent on pluviosity. Alonso et al. (2005) present an example of the relation between pluviosity and water pressure measured in the rockfill on a review of the behaviour of Beliche Dam, as Figure 4.9 shows.

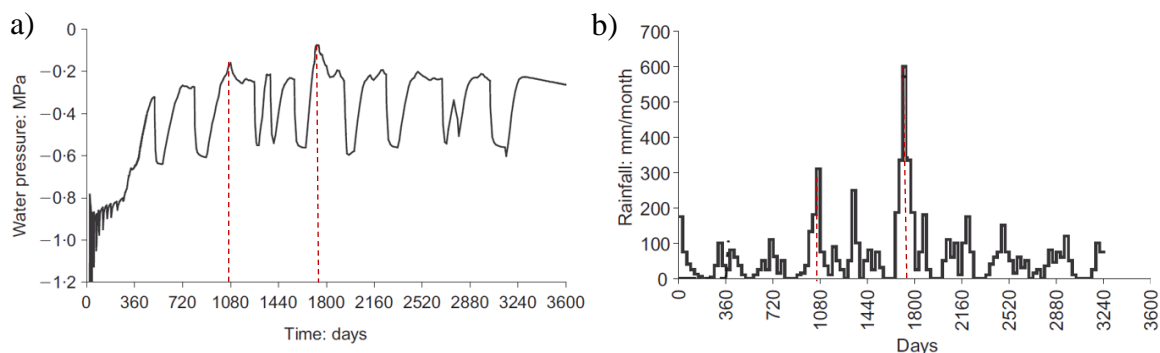


Figure 4.9 - a) variation of water pressure and b) monthly precipitation recorded in Beliche Dam over time (adapted from Alonso et al., 2005).

It is possible to notice that the lowest values of suction recorded in the rockfill were associated to the highest precipitation periods, strengthening the idea that measuring precipitation can give

an efficient perception of water pressure in the embankment, especially on impervious faced dams, where there is no percolation associated to the reservoir.

Beliche Dam is a structure known for recording significant wet-induced collapse, caused by impoundment and intense precipitation. That construction has been broadly studied over the years because it holds a large amount of large-scale laboratory tests and a very complete field monitoring system (Alonso et al., 2005). RCM demonstrated a qualitative behaviour very similar to that structure, especially regarding how their vertical displacements reacted to intense pluviosity. Figure 4.10 presents the settlement measured on the crest of the embankment of Beliche Dam and the recorded pluviosity. Figure 4.10 presents the settlement measured on the crest of the embankment of Beliche Dam and the recorded pluviosity.

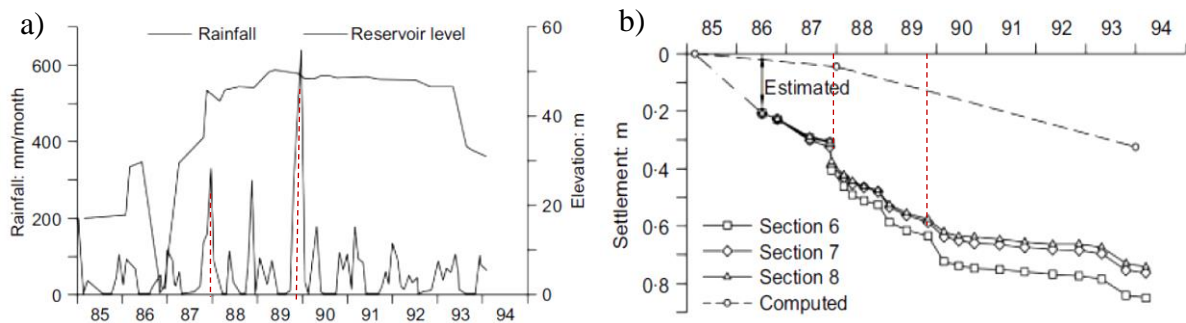


Figure 4.10 - a) rainfall intensity and reservoir level after dam construction and b) vertical settlements registered at crest marks on Beliche Dam (adapted from Alonso et al. 2005).

It is possible to notice a significant resemblance between the settlement curves presented for RCM and for Beliche Dam. The shape of the curves is qualitatively very similar for the two structures, with curves tending to logarithmic relations being successively disrupted by moments of abrupt settlements, followed by periods in which this trend is repeated. The moments of collapse in the two constructions are comparable as well, being coincident to the maximum records of rainfall in both cases. This parallelism between these two rockfill dams supports the conclusion that the abrupt settlements recorded in RCM were caused by wet-induced collapse.

Concluding that collapse due to wetting is the mechanism responsible for the settlements recorded in RCM suggests that Rings 1 and 2, which do not show any relevant abrupt deformation, probably have reached very low values of suction (perhaps even zero) at least once, probably in the beginning of the embankment's life. That proposition cannot be confirmed, but these are the rings located at the lowest elevation in the rockfill, placing them closer to the ground water table. Rings 1 and 2 are also further from the atmosphere, being less subject to evaporation in dry periods than the more superficial rings.

4.2. Horizontal displacements in the rockfill

Although the evaluation of the horizontal displacements is not the primary objective of this study, a complete analysis of the behaviour of the rockfill inevitably includes an assessment of the horizontal movements recorded in the embankment. Figure 4.11 shows the horizontal displacements registered in Inclinator IB3, installed in section PO3 (Figure 3.14 and Figure 3.15). The results are presented for direction A, perpendicular to the crest alignment (positive values refer to movements towards downstream). Direction B have not demonstrated significant deformation or any relevant trend, therefore will not be considered.

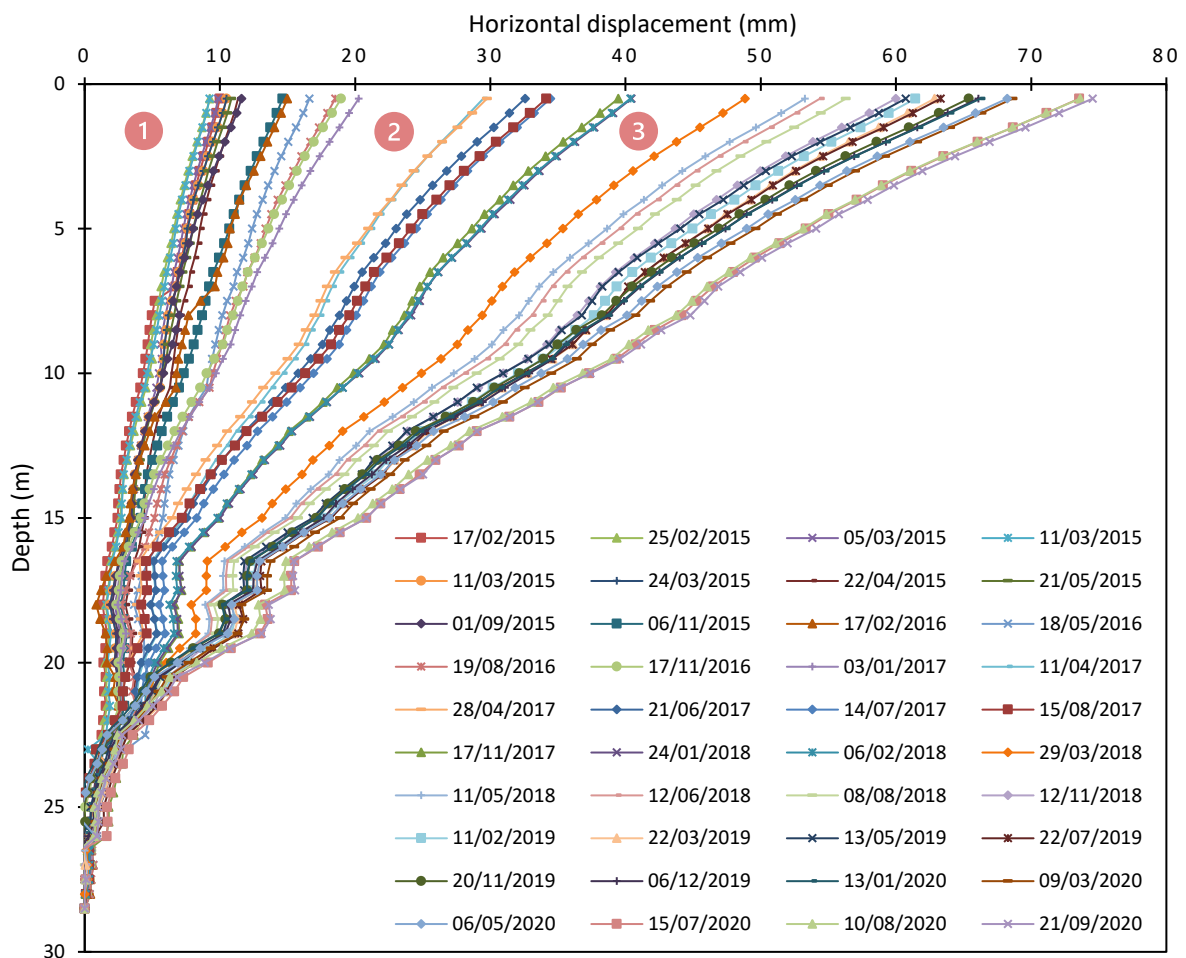


Figure 4.11 - Horizontal displacements recorded in Inclinator IB3, direction A.

The 3 moments of collapse are marked in the graph, showing that horizontal displacements also increased substantially in the analysed moments. The global aspect of the curves suggests a typical behaviour of an inclinometer installed in the embankment of a dam. Analyses of the horizontal displacements of Rings 3 to 9 are presented in Figure 4.12 (with water level in the

reservoir) and Figure 4.13 (with precipitation), in which their horizontal movements were estimated from the measurement points in Inclinator IB3 with the closest elevation to the rings. Two records were removed from this analysis due to the strange values, indicating probable misreadings.

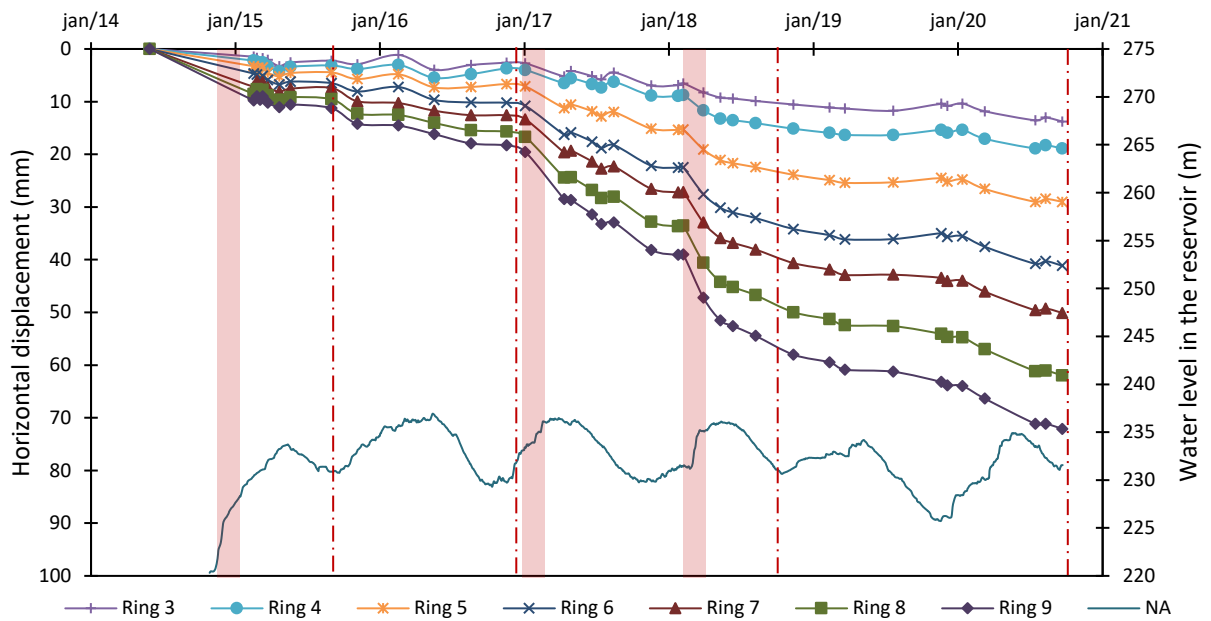


Figure 4.12 - Horizontal displacements of the extensometers and water level in the reservoir.

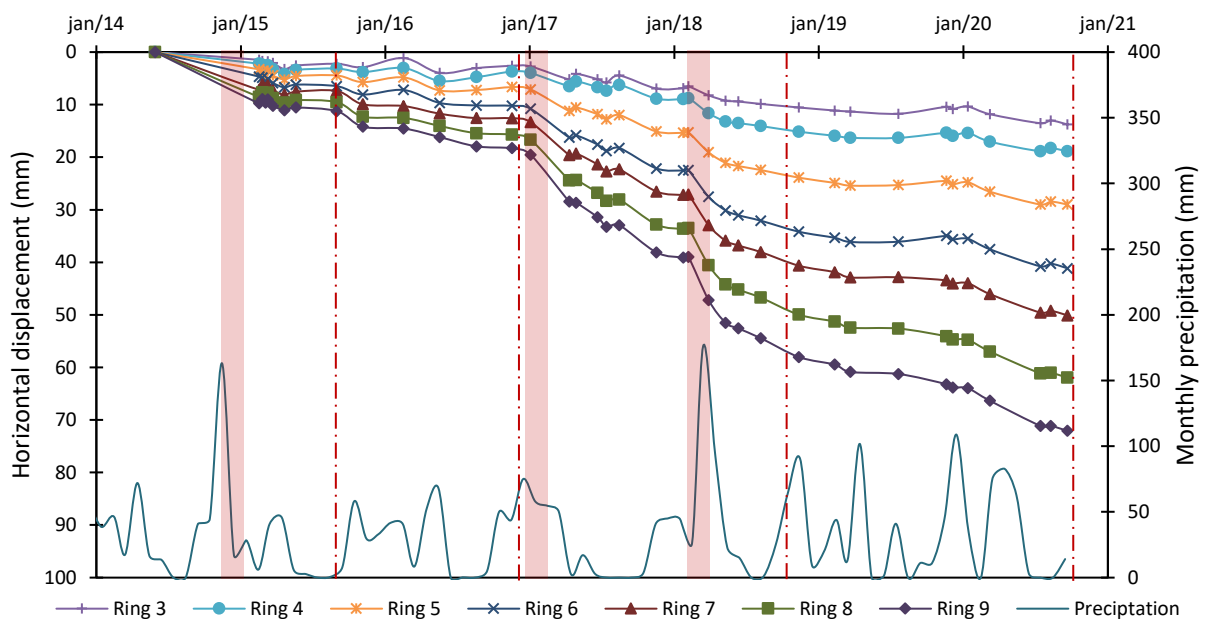


Figure 4.13 - Horizontal displacements of the extensometers and monthly precipitation.

From Figure 4.12 and Figure 4.13, it is possible to conclude that, in the moments of wet-induced collapse, the horizontal movements essentially follow the same behaviour registered for the vertical displacements. Therefore, all considerations made regarding the association of settlements and water level in the reservoir or pluviosity can be considered valid for the horizontal movements as well. The moments of collapse 2 and 3 are quite evident, and although before collapse 1 there had been only the initial measurement 8 months earlier, the horizontal displacements registered next are substantial, suggesting that a collapse could have happened.

Apart from the significant effect the collapses have in the displacements, the influence of the variation of the water level in the reservoir in the horizontal movements is evident. Between September of 2015 and November of 2016, and October of 2018 and September of 2020 (delimited by the dashed lines), it is possible to see how the rockfill respond to the oscillation of the reservoir in terms of horizontal displacements. Although reduced when compared to the elevated values measured in the moments of collapse deformation, the horizontal displacements show a trend of return associated to partial drawdown and increase due to new elevation. This smaller level of deformation is expected, since the repeated oscillations in the reservoir are not expected to cause new plastic strains. Table 4.3 presents the values of effective horizontal stress estimated by the numerical model created during the design phase.

Table 4.3 - Horizontal effective stress calculated in section PO3.

| | Effective horizontal stress (kPa) | | |
|-----------------|-----------------------------------|--------------------|-----------|
| | Before filling | Normal water level | Variation |
| Datum - Ring 1 | 222,7 | 226,9 | +1,9% |
| Ring 1 - Ring 2 | 183,9 | 193,4 | +5,2% |
| Ring 2 - Ring 3 | 141 | 155,1 | +10,0% |
| Ring 3 - Ring 4 | 102,4 | 120,2 | +17,4% |
| Ring 4 - Ring 5 | 75,6 | 94,8 | +25,4% |
| Ring 5 - Ring 6 | 57,5 | 75,7 | +31,7% |
| Ring 6 - Ring 7 | 44,1 | 60 | +36,1% |
| Ring 7 - Ring 8 | 36,4 | 46,6 | +28,0% |
| Ring 8 - Ring 9 | 36,8 | 40,2 | +9,2% |

Differently from the vertical stress (Table 4.1), which is only marginally influenced by the water level in the reservoir, the increase in horizontal stress due to impoundment is quite significant. When not overlapped by the substantial strains associated to the collapses, the horizontal movements in the embankment appear to be influenced by the variation in the load due to the water. It is also possible to notice in the curves the superposition of secondary deformation and

movements associated to this oscillation. Pluviosity, on the other hand, apparently does not have any effect in the horizontal displacements, besides the moments of collapse.

Figure 4.14 brings the relation between horizontal and vertical displacements. The proportion of horizontal and vertical movements increases as depth decreases, reflecting that, in the alignment of Inclinator IB3, the rotation of the principal stresses due to the water load is more significant closer to the surface.

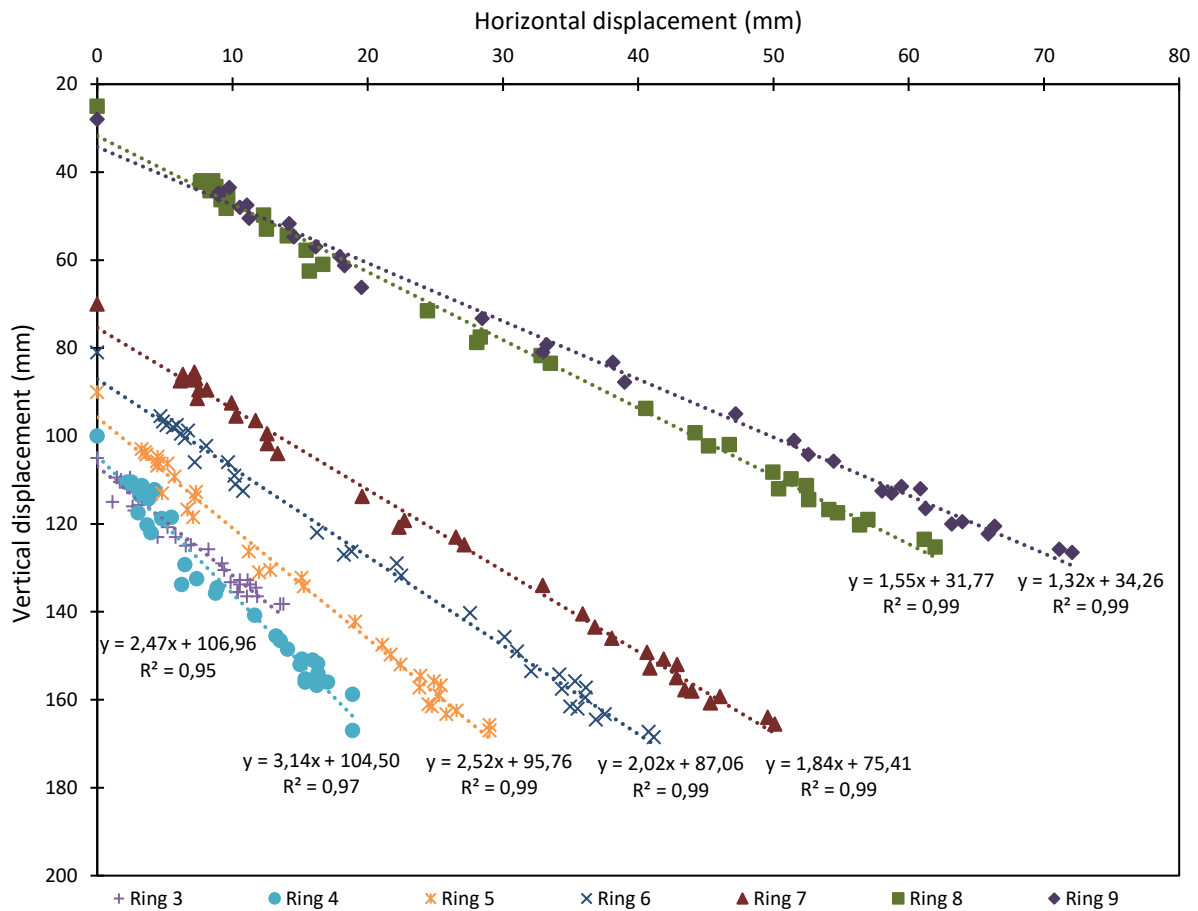


Figure 4.14 - Vertical and horizontal displacements of the extensometers.

From the analyses of horizontal movements in Inclinator IB3, it is evident that the collapses due to wetting have considerable influence on the horizontal movements of the embankment. Nevertheless, in the periods distant from these abrupt deformations, the effect of the oscillation in the water level is noticeable, though reduced.

4.3. Time-dependent deformation in the rockfill

Secondary deformation in rockfill can be explained, in a simplified manner, as a delayed breakage of the particles under constant load, followed by a rearrangement of the smaller fragments in the voids, enhancing density of the material (Oldecop and Alonso, 2007). As in most geotechnical materials, long-term strains are related to the logarithm of time (Hunter and Fell, 2002; Kermani, 2016). However, when evaluating deformations of a rockfill dam, there is not an agreement regarding what should be considered the beginning of the process. Hunter and Fell (2002), for instance, proposes a relation in which the time datum is the end of construction, while Kermani (2016) suggests that it should be when the impoundment is finished and the stress state inside the dam body reaches a more stable condition.

The recommendation of Kermani (2016), which follows the same concept used for oedometer tests with load increment (time is reset every new stage), will be adopted in this study. The proposition that when the stress state changes significantly in the rockfill a new time datum is set for secondary deformation suits properly the behaviour observed in the extensometers. The difference is that, in the current analysis, the factor altering the stress state is not an increase in load, like suggested by Kermani, but a decrease in suction. Nevertheless, the concept remains, since both alters the effective stress state and, consequently, the yield surface, causing plastic strains in the rockfill.

The analysis presented in the last sections suggests that RCM experienced three moments of abrupt plastic deformation between December of 2013 and September of 2020. Since the precise moment when each wet-induced collapse occurred cannot be defined, setting the correspondent time datum for a long-term deformation analysis is not a direct task in this case. Therefore, a criterion had to be defined, and the days in each interval when the accumulated precipitation surpassed the previous maximum were chosen to be considered the moments when collapses occurred, as presented in Table 4.4.

Table 4.4 - Time datum defined for each wet-induced collapse.

| Collapse | Time datum | Accumulated precipitation | Previous maximum |
|----------|------------|---------------------------|------------------|
| 1 | 28/11/2014 | 238 mm | 223 mm |
| 2 | 12/02/2017 | 271 mm | 249 mm |
| 3 | 30/03/2018 | 333 mm | 332 mm |

When a new yield surface is defined (and no other relevant modification in the stress state occurs), secondary deformation is expected to start in the material. Figure 4.15, Figure 4.16 and Figure 4.17 present the relation between vertical strains of the rockfill and time for each of the periods between collapses, considering the time datums defined in Table 4.4. Deformation is presented for the total thickness of rockfill under each extensometer, calculated as vertical displacement measured in the ring divided by total thickness of embankment beneath that point.

For the three analysed periods, it is possible to notice the expected linear relations between deformations and the logarithm of time in the seven magnet rings considered in the study. Nevertheless, the relations only present this characteristic when time is reset after each collapse, supporting the proposition that a new time datum for secondary deformation is set after each significant plastic deformation.

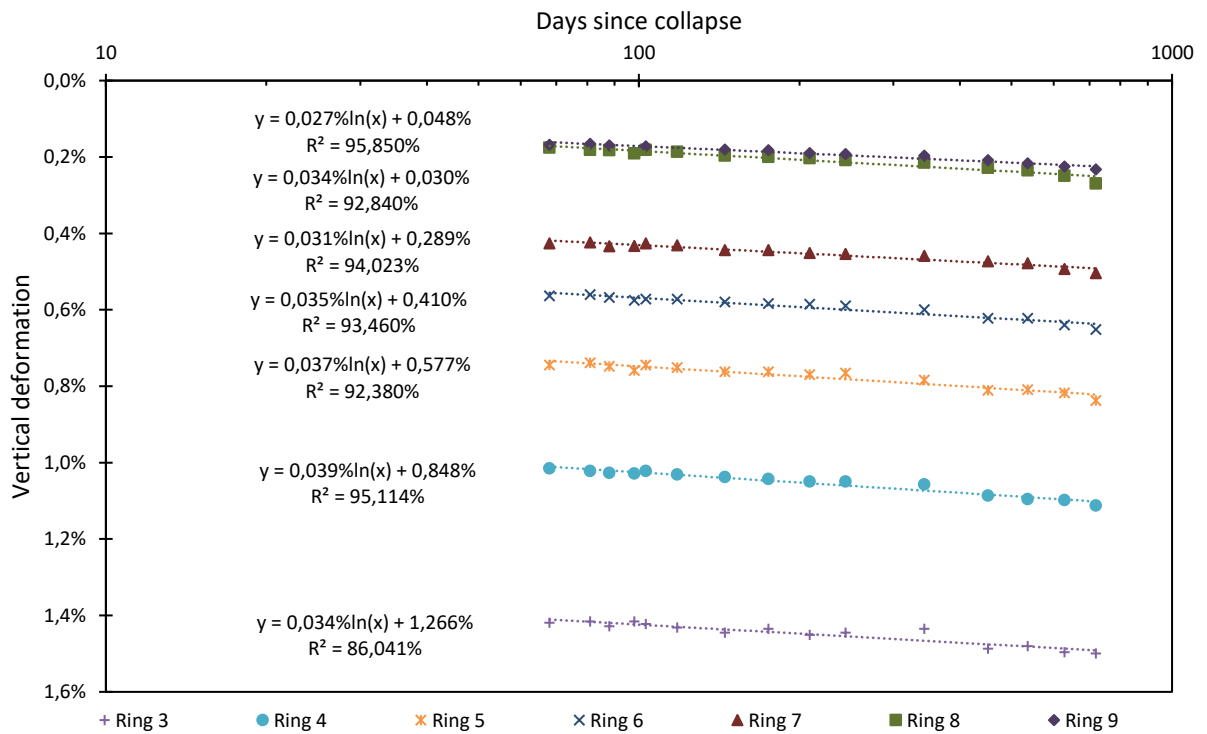


Figure 4.15 - Vertical deformation of the rockfill in each extensometer for the period between collapses 1 and 2.

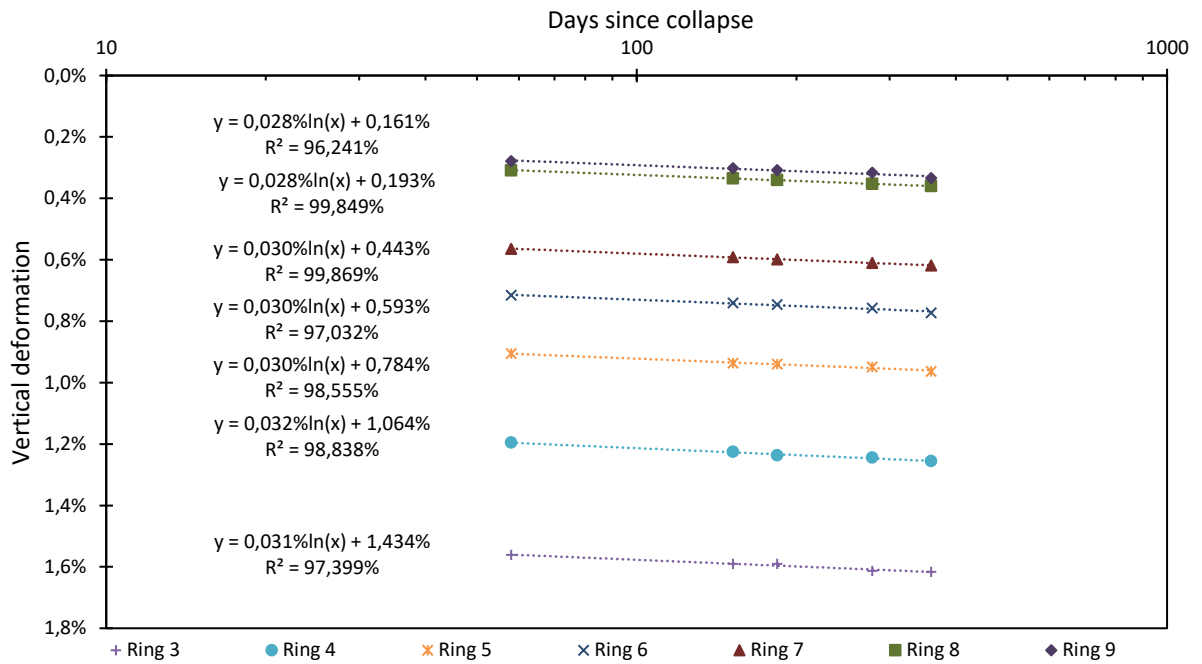


Figure 4.16 - Vertical deformation of the rockfill in each extensometer for the period between collapses 2 and 3.

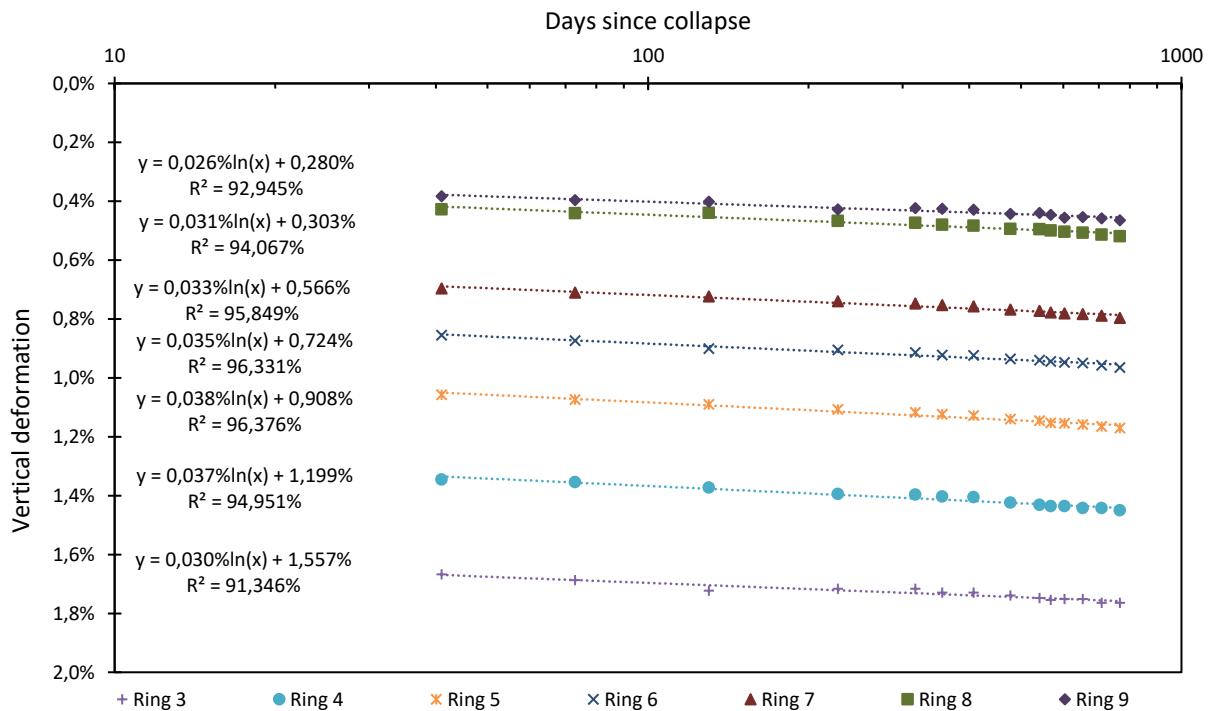


Figure 4.17 - Vertical deformation of the rockfill in each extensometer for the period between collapse 3 and September 2020.

Hunter and Fell (2002) and Kermani (2016) suggest estimations for the rate in which time-dependent settlement occurs in the crest of a rockfill dam. To compare the strains recorded in RCM with the proposition of these authors, the extensometer with the highest elevation, Ring 9, was considered to be representative of the behaviour of the dam crest. Both studies suggest a rate of long-term deformation (settlement as percentage of height per logarithm of cycle of time) based on the strength of the rock and the height of the embankment. The greywacke used in the rockfill is classified as a high strength rock, according to AS 1726-1993 (classification considered by both studies) due to its unconfined compressive strength, as presented in Table 3.5. The height of the embankment in the section of analysis is approximately 30 meters. Table 4.5 presents the results for Ring 9 (obtained from Figure 4.15, Figure 4.16 and Figure 4.17). In Figure 4.18 and Figure 4.19, it is possible to see these results plotted in the propositions of Hunter and Fell (2002) and Kermani (2016), respectively.

Table 4.5 - Vertical deformation rate of Ring 9

| Period | Vertical deformation rate of Ring 9 |
|-----------------------------|--|
| Collapse 1 - Collapse 2 | 0.027% In cycle of time (0.062% log ₁₀ cycle of time) |
| Collapse 2 - Collapse 3 | 0.028% In cycle of time (0.065% log ₁₀ cycle of time) |
| Collapse 3 - September 2020 | 0.026% In cycle of time (0.061% log ₁₀ cycle of time) |

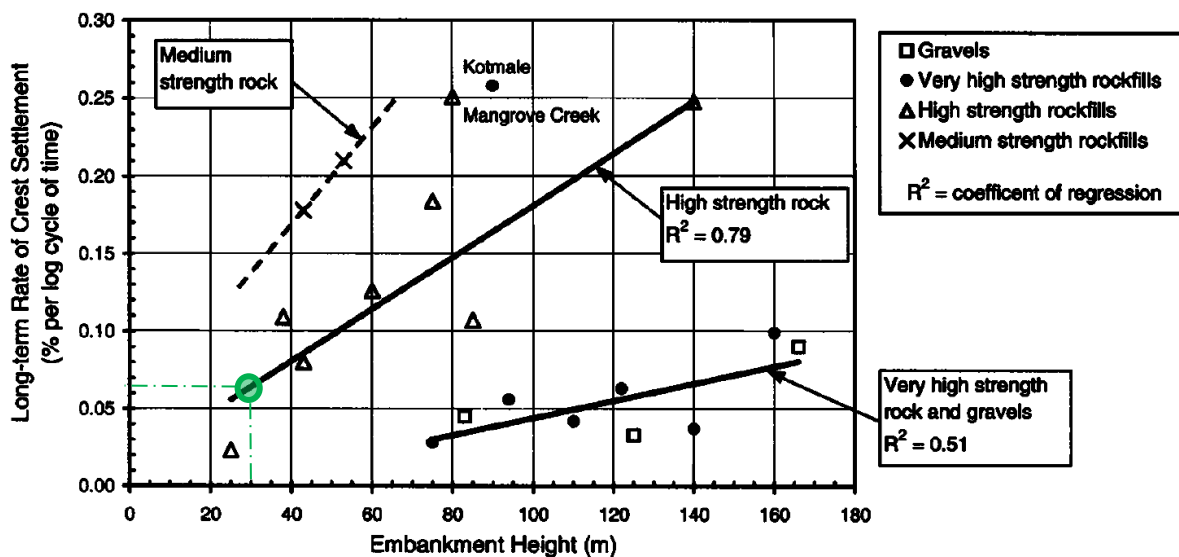


Figure 4.18 - Long-term settlement rate of Ring 9 plotted in Hunter and Fell's proposition (adapted from Hunter and Fell, 2002).

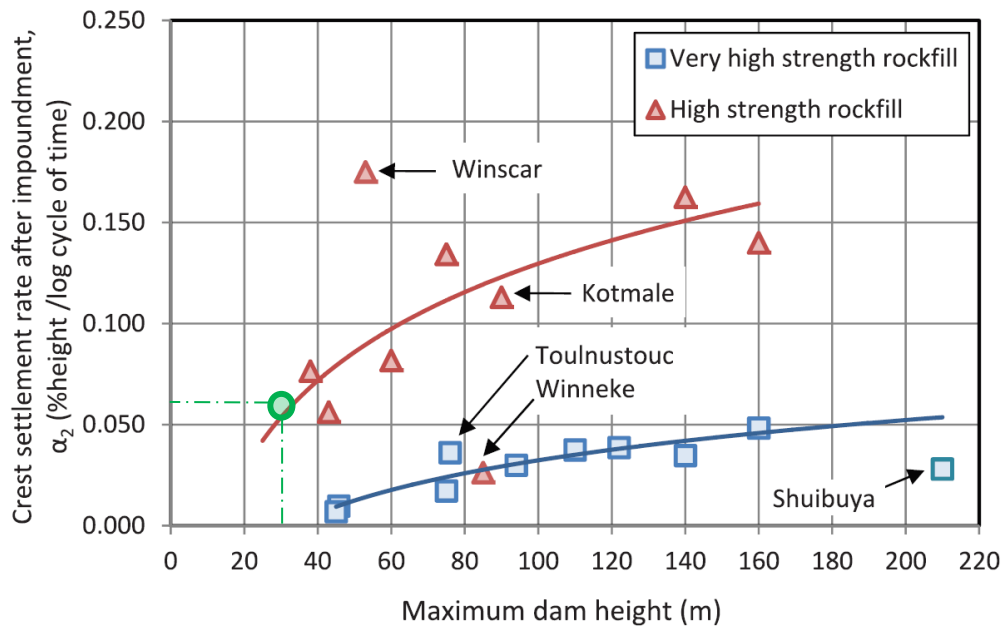


Figure 4.19 - Long-term settlement rate of Ring 9 plotted in Kermani's proposition (adapted from Kermani, 2016).

Both propositions give very similar estimations for embankments with the characteristics of RCM, with settlement rates close to 0.06% of embankment height per \log_{10} of cycle of time. As it is possible to notice, the settlement rates calculated for Ring 9 suit adequately both estimations, leading to the conclusion that the time-dependent strains observed in the rockfill are, so far, as expected.

Figure 4.20 presents, in the left vertical axis, the long-term deformation rate after each collapse for the seven extensometers considered in this study, and in the right vertical axis, the total post-construction deformation. The extensometers located at the central part of the section present a tendency to show larger time-dependent deformation rates than the extensometers situated closer to the crest. Nevertheless, the reference values aforementioned relate to the crest, not the internal part of the rockfill embankment. Therefore, it might be more adequate to keep the comparison with these reference values limited to Ring 9, already discussed and presented in Figure 4.18 and Figure 4.19.

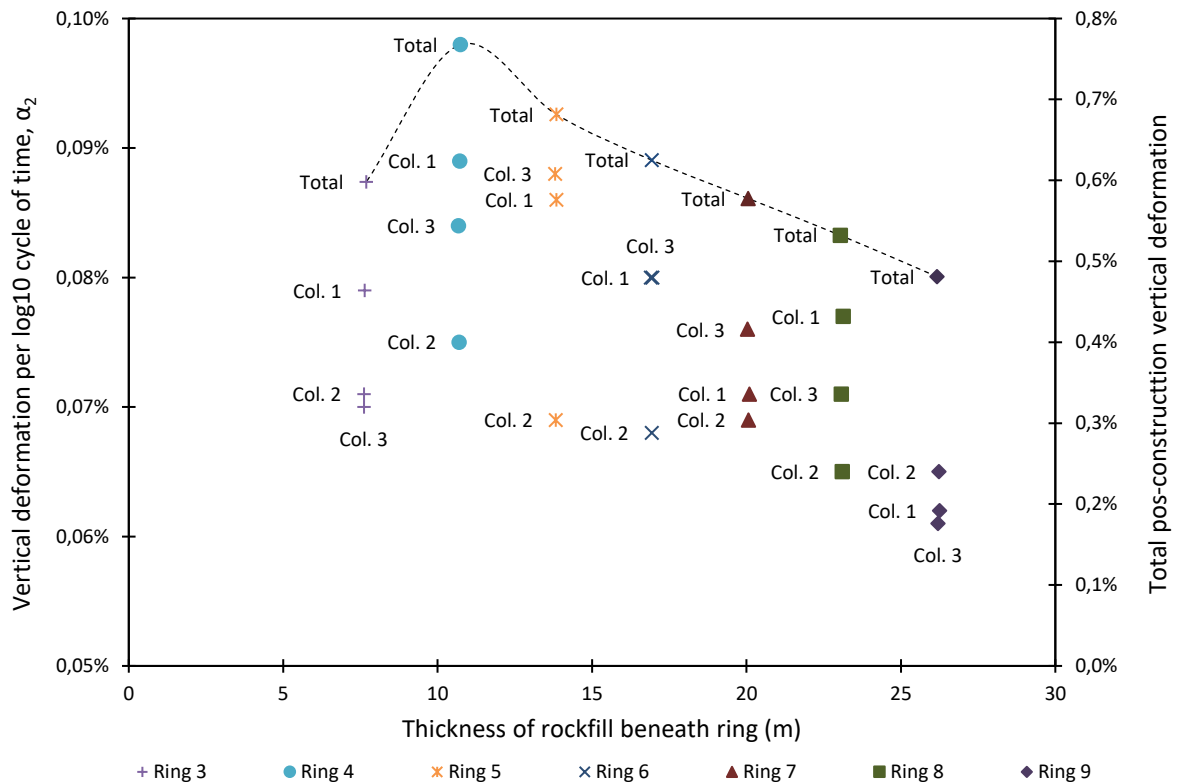


Figure 4.20 - Long-term settlement rate for extensometers 3 to 9 after each collapse.

For what regards the horizontal movements in the embankment, it is not possible to determine which fraction of the measurements in the inclinometer actually refers to deformation of the rockfill. Therefore, the long-term analyses conducted in this study concern to horizontal displacements, considering the same time datum presented in Table 4.4. Figure 4.21, Figure 4.22 and Figure 4.23 present the relation between horizontal displacement of the extensometers and time for each of the three analysed periods. It is possible to notice the influence of the variation in the water level on the regressions, showing more dispersion in the measurements when compared to the relations for vertical displacements. Nevertheless, the overall trends are evident, especially for the second and third periods.

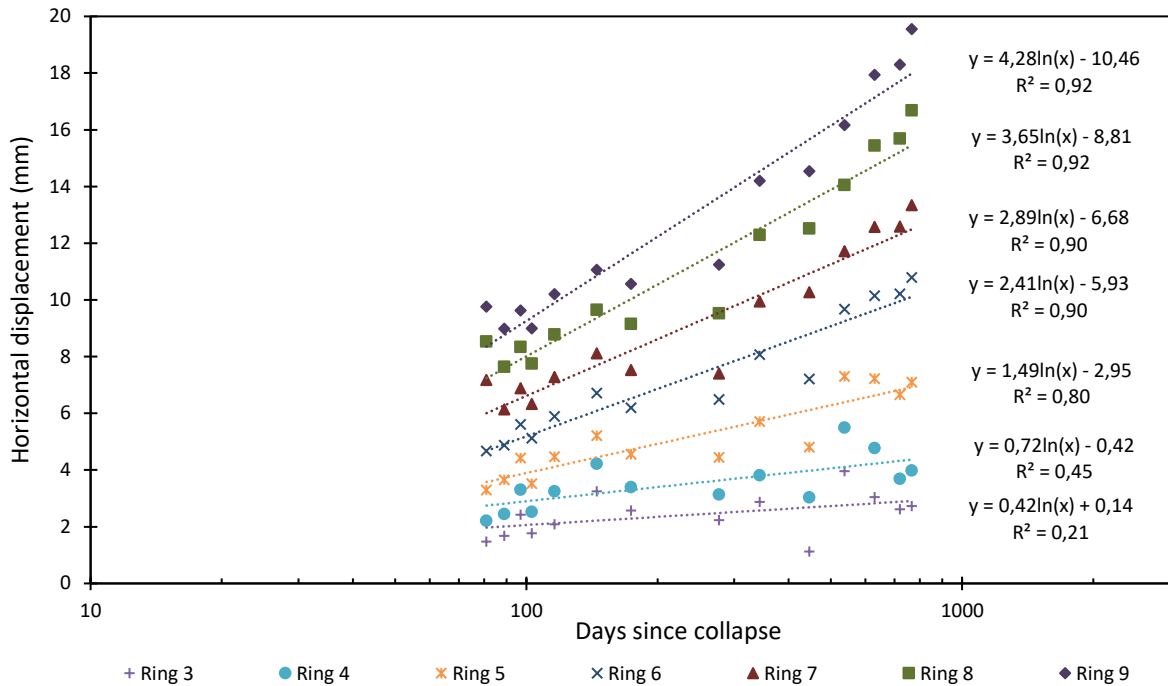


Figure 4.21 - Horizontal displacements for the period between collapses 1 and 2.

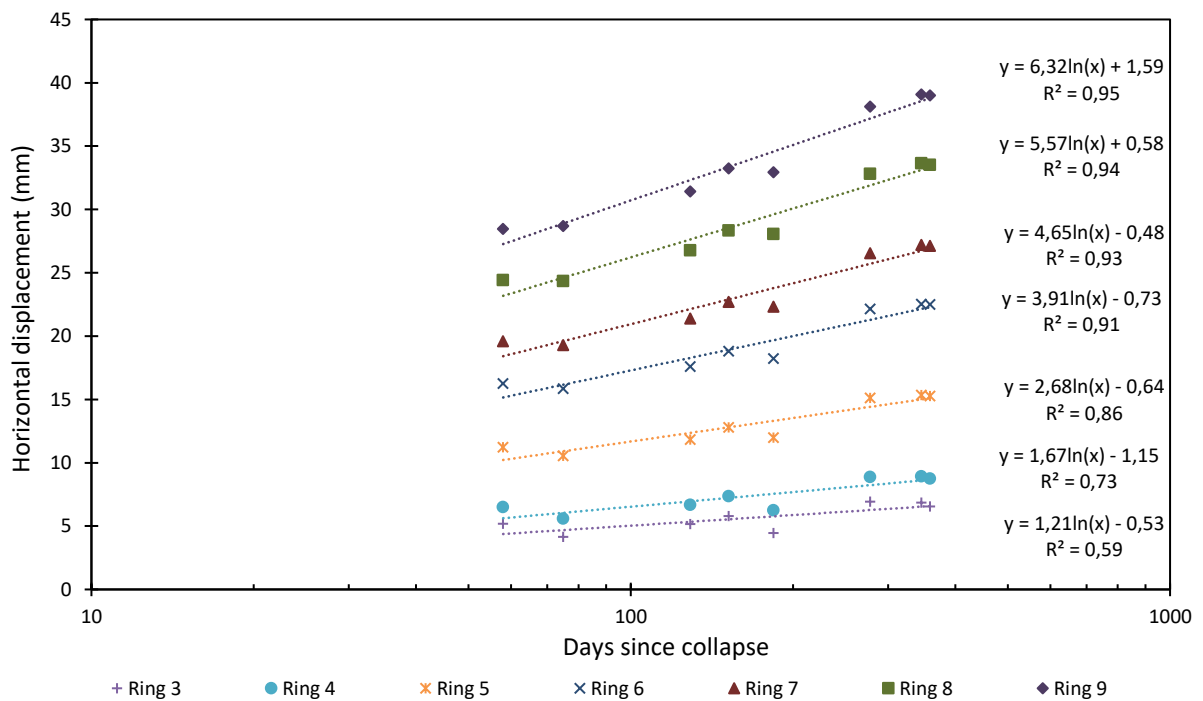


Figure 4.22 - Horizontal displacements for the period between collapses 2 and 3.

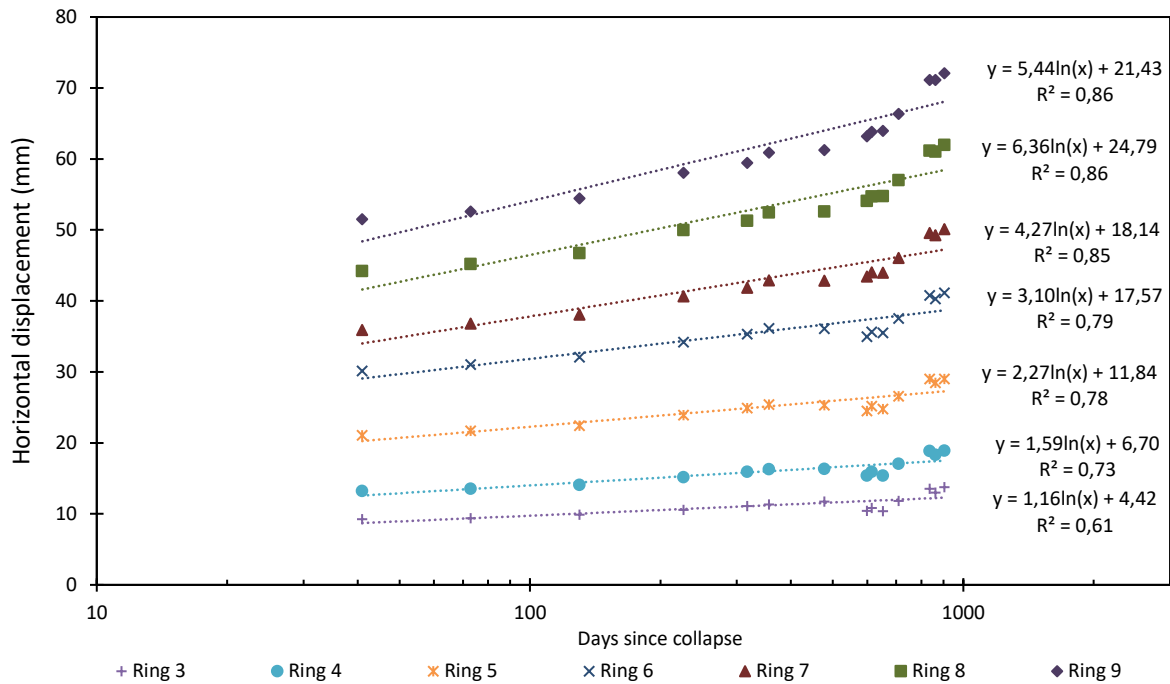


Figure 4.23 - Horizontal displacements for the period between collapse 3 and September of 2020.

Table 4.6 presents the horizontal displacement rates estimated for all rings analysed. As expected, the highest movement rates are estimated for the points closer to the crest of the embankment. Table 4.7 present these values normalized by thickness of rockfill beneath each extensometer.

Table 4.6 - Horizontal displacement rates in the extensometers.

| | Horizontal displacement rate (mm / ln cycle of time) | | |
|--------|--|----------------------------|-----------------------------------|
| | Collapse 1 - Collapse 2 | Collapse 2 - Collapse 3 | Collapse 3 - September of 2020 |
| Ring 3 | 0,42 | 1,21 | 1,16 |
| Ring 4 | 0,72 | 1,67 | 1,59 |
| Ring 5 | 1,49 | 2,68 | 2,27 |
| Ring 6 | 2,41 | 3,91 | 3,1 |
| Ring 7 | 2,89 | 4,65 | 4,27 |
| Ring 8 | 3,65 | 5,57 | 5,44 |
| Ring 9 | 4,28 | 6,32 | 6,36 |

Table 4.7 - Horizontal displacement rates in the extensometers normalized by thickness of rockfill.

| | Normalized horizontal displacement rate (mm / ln cycle of time / m) | | |
|--------|--|----------------------------|-----------------------------------|
| | Collapse 1 - Collapse 2 | Collapse 2 - Collapse 3 | Collapse 3 - September of 2020 |
| Ring 3 | 0,05 | 0,16 | 0,15 |
| Ring 4 | 0,07 | 0,15 | 0,15 |
| Ring 5 | 0,11 | 0,19 | 0,16 |
| Ring 6 | 0,14 | 0,23 | 0,18 |
| Ring 7 | 0,14 | 0,23 | 0,21 |
| Ring 8 | 0,16 | 0,24 | 0,23 |
| Ring 9 | 0,16 | 0,24 | 0,24 |

Fell et al. (2015) compiled the values of post-construction horizontal movements recorded in the crest of several rockfill dams with impervious face. Table 4.8 show the results presented by those authors, along with the records of RCM. The detailed behaviour of those dams through time, however, is not provided, making impossible to evaluate their general performance and compare with RCM (such as form of the curves and rate of movement through the logarithm of time). Nevertheless, it is possible to compare the total horizontal displacement rate, assuming a linear relation and normalizing by the height of the embankment.

The estimated horizontal displacement rate of RCM appears to be an intermediate value (0.41 mm/year/m) among the analysed dams (0.01 – 1.02 mm/year/m). The heights of the embankments and the time spans of observation varies significantly, thus the estimated rates also comprises a very large range of values. It is pertinent to notice the considerable dispersion of results, without clear trends between the rate of horizontal displacement and height of dam (Figure 4.24) or time span of observation (Figure 4.25). Additionally, none of the dams in that list present the same conditions of RCM regarding height and period of observation, with Lower Bear 2 (0.63 mm/year/m) representing the closest situation, but still not similar enough for a direct comparison. Another important point to mention refers to the tendency that long-term deformations have to reduce in time. By assuming linear relations, it is expected that the larger the period of observation of, the smaller the displacement rate. Therefore, it might not be adequate to compare the estimated rate of RCM with others specifically, but, as an alternative, conclude that the result is in the array of records of other dams, showing no evident sign of problem in that matter.

Table 4.8 - Horizontal displacement of the crest of rockfill dams with impervious face (After Fell et al., 2015).

| Dam Name | Height (m) | Horizontal displacement (mm) | Time span (years) | Normalized rate of horizontal displacement (mm/year/m) |
|----------------|-------------|------------------------------|-------------------|--|
| RCM | 28.5 | 74.6 | 6.3 | 0.41 |
| Bastyan | 75 | 16 | 7.5 | 0.03 |
| Brogo | 43 | 35.7 | 18.25 | 0.05 |
| Cethana | 110 | 83 | 22 | 0.03 |
| Dix River | 84 | 970 | 32 | 0.36 |
| Foz do Areia | 160 | 248 | 6 | 0.26 |
| Golillas | 125 | 7 | 6 | 0.01 |
| Kangaroo Creek | 60 | 50 | 10 | 0.08 |
| Kotmale | 90 | 62 | 2.5 | 0.28 |
| Lower Bear 1 | 75 | 305 | 4 | 1.02 |
| Lower Bear 2 | 46 | 116 | 4 | 0.63 |
| Mangrove Creek | 80 | 196 | 15 | 0.16 |
| Murchison | 94 | 22 | 12 | 0.02 |
| Reece | 122 | 68 | 7.5 | 0.07 |
| Salt Springs | 100 | 550 | 27 | 0.20 |
| Scotts Peak | 43 | 190 | 17 | 0.26 |
| Serpentine | 38 | 38 | 21 | 0.05 |
| Shiroro | 125 | 27 | 1.5 | 0.14 |
| Xingo | 140 | 320 | 5.2 | 0.44 |

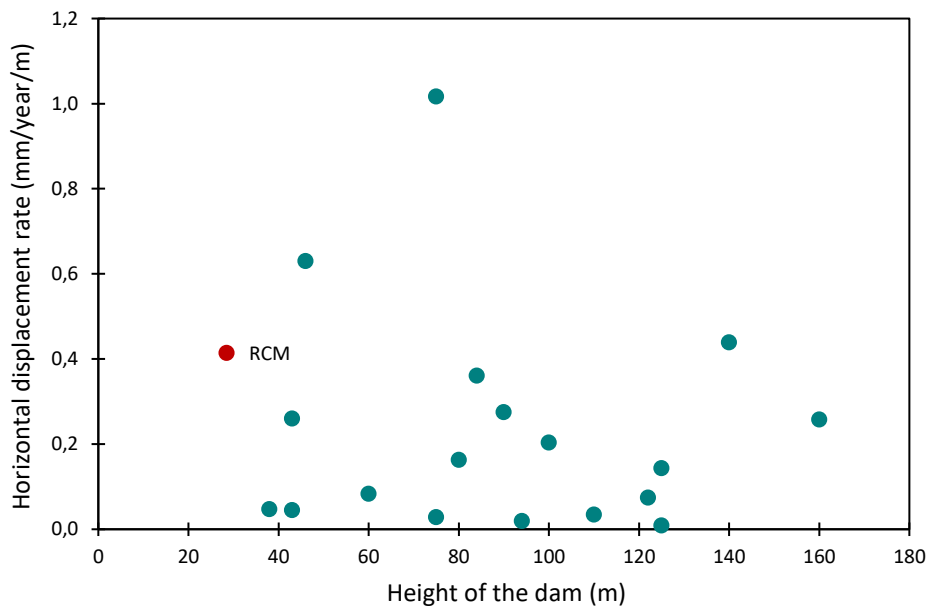


Figure 4.24 - Relation between horizontal displacement rate and height of the embankment of the dams (after Fell et al., 2015).

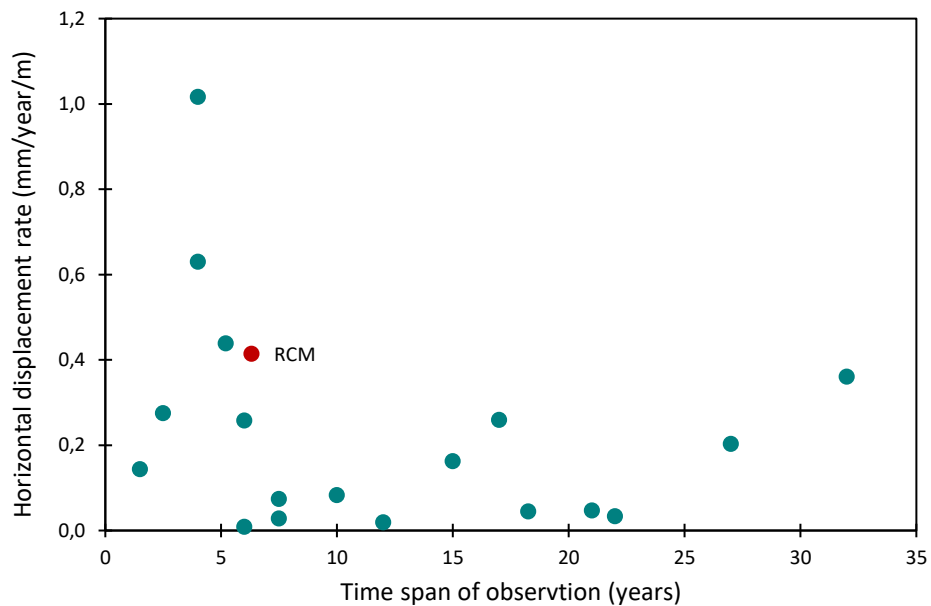


Figure 4.25 - Relation between horizontal displacement rate and time span of observation of the dams (after Fell et al., 2015).

5. Conclusions

5.1. Summary and conclusions of the study

The main objective of this study was to identify and understand the reasons that led the rockfill embankment to present 3 moments when unexpected abrupt settlement occurred, and to assess if these movements should be treated as a symptom of a problem in the dam. Complementarily, evaluations of the long-term deformation rates registered in the embankment and horizontal displacements were also executed.

To define the causes of the vertical displacements, it was necessary to assess the records of the extensometers installed in the main section of the embankment. The possible influences of the environmental aspects considered (water level in the reservoir and pluviosity) were evaluated, permitting to set relations between these factors and the deformation, including verifying the simultaneousness of the events.

These analyses aforementioned, presented in Chapter 4, allowed to conclude that the mechanism responsible for the unexpected deformations registered in the rockfill was wet-induced collapse. The main arguments to support this proposition are based on the fact that all collapses recorded were associated to a new maximum in the precipitation historical series, and every time a new maximum was registered, a collapse occurred. In addition to that, the general behaviour registered by the extensometers in RCM rockfill were very similar to typical deformation curves of rockfill upon wetting, as presented in the literature review. The comportment of at least other two dams affected by wet-induced collapse (Beliche and Martín Gonzalo dams) significantly resembled the observations on RCM, especially Beliche Dam, a structure deeply studied through the years.

Besides the fact that various evidences suggest that the mechanism responsible for the increase in the settlements rates was associated to the pluviosity, it was yet necessary to examine the possible influence of the fluctuations of the water level in the reservoir. This evaluation permitted to conclude that these oscillations represented a small change in the vertical stress in the extensometers section, making improbable the association of these events to the abrupt settlements. In addition to that, unload-reload cycles should register smaller strains, since the material is expected to be stiffer. Moreover, no collapse was recorded when the water level reached its maximum, and the extensometers never registered swell associated to the reduction of load due to partial drawdowns of the reservoir. All these evidences support the conclusion

that the influence of the variations of the water level in the reservoir is probably very reduced, if existent.

Therefore, the findings of the central aspect of the study – the characterization of the mechanism responsible for the collapses – may be considered satisfactory. The nature of the phenomenon is in line with the behaviour observed in similar dams and does not indicate a clear sign of imminent risk for the structure. The literature review presented suggest that, in most cases, potential subsequent problems associated to these vertical deformations in rockfill dams, when existent, are related to serviceability, not failure of the structure. Nevertheless, monitoring all the instruments installed in the embankment and adjacent areas is essential to guaranty that the structure continues to perform adequately.

Regarding the global deformation of the embankment, the relations between vertical and horizontal displacements and depth of the extensometers showed an expected overall performance. The inclinometer existent in the Section PO3 demonstrated substantial increases in the horizontal movements in the same moments that abrupt settlements were recorded in the extensometers, suggesting that wet-induced collapse causes strains in both directions. The relation between vertical and horizontal displacements in the extensometers follows what is expected for an embankment subject to water load, such RCM.

Differently from what concerns the vertical displacements, measurements in Inclinometer IB3 showed that fluctuations in the water level have some influence in the horizontal movements of the rockfill. Rises in the reservoir are coincident with increases in the horizontal displacements rates, as well partial drawdowns are followed by reduction in the movements rates, eventually even indicating some recuperation in the displacements. However, this influence is only perceptible in the periods when no collapses occur, since the mechanisms are overlapped and the displacements due to plastic strains are considerably larger. Secondary horizontal deformation is recorded as well, being responsible for a tendency of continuous movement in the downstream direction.

Regarding the long-term settlement rates recorded in the rockfill, it is possible to conclude that the extensometer representing the crest of the embankment presented a vertical deformation rate close to $0.06\% \log_{10}$ of cycle of time, quite similar to predictions based on the behaviour of other impervious-faced rockfill dams. Continuing on this subject, the proposition that a new time datum is set after each collapse appeared to be adequate, based on the theory behind it as well on the records of the extensometers. Nevertheless, it shall be mentioned that the time spans available for these measurements are reduced when examining long-term deformations, and more appropriate conclusions should be carried after a longer period of monitoring.

5.2. Final considerations

The evidences supporting that wet-induced collapse is the mechanism responsible for the settlement in the rockfill might be considered strong. Besides being reasonable, associating the increase in moisture in the rockfill with periods of high precipitation is not new in geotechnical engineering and is considered a consistent relation. However, for this phenomenon to be undoubtedly characterized, there has to be a systematic record of the humidity in the rockfill voids, which is not currently existent. Consequently, it is not possible to determine whether a new collapse could possibly occur nor when, since the results were obtained by association to pluviosity, not direct measurements.

The possibility of having more wet-induced collapses only ceases when the rockfill reaches 100% of relative humidity for the first time (not necessarily associated to a flooding of the rockfill). Therefore, without knowing which values of suction have already been reached, it is not possible to determine if another event might occur. However, from the past records of hydrological data, it is possible to have an estimation of how large (in a historical sense) the precipitation events that caused collapse were, and what would be the return period of a larger event. A rainfall frequency analysis might provide an estimation of the chances of a new maximum to occur in the next years, possibly resulting in a new wet-induced collapse.

On the other hand, although predicting when a new period will record a rainfall event that surpasses all the previous events might give an estimation, the relation is not so direct. Other aspects have great influence in the humidity present in the rockfill, such as evaporation. For instance, if a period of intense pluviosity follows a long drought or is associated to higher temperatures, a new minimum in suction might not be reached. Therefore, the confirmation that a new wetting collapse is impossible to occur again is very complex and involves a critic and broad engineering judgement.

5.3. Recommendation for further analysis

As stated in the previous section, although a frequency analysis of rainfall data cannot provide a definitive answer whether wet-induced collapse could occur again, it is the most reliable projection available in this case. In addition, it constitutes a relatively simple analysis, eventually already existent considering RCM is part of a mining compound. Therefore, it might be fruitful to proceed with this evaluation.

Regarding the characterization of the materials, the phenomena of collapse induced by wetting and creep deformation might be deeper investigated with laboratory tests conducted in samples

collected in the rockfill. The findings should provide valuable information to assess how the behaviour recorded in the field compares to the tests in controlled conditions. In addition, the results of laboratory tests might be used to determine input parameters for numerical modelling of the structure. For what concerns the instrumentation of the embankment, the installation of sensors for suction measurement and vibrating wire piezometers in the embankment body would provide important information regarding the humidity existent in the rockfill.

References

Alaei, E., Mahboubi, A. (2012). “A discrete model for simulating shear strength and deformation behaviour of rockfill material, considering the particle breakage phenomenon”. *Granular Matter*, Vol. 14, Issue 6, pp.707-717.

Alonso, E., Gens, A., Josa, A. (1990). “A constitutive model for partially saturated soils”. *Géotechnique*, Vol. 40, Issue 3, pp. 405-430.

Alonso, E, Oldecop, L. (2000). “Comportamiento de pedraplenes y escolleras. Simposio sobre Geotecnia de Infraestructuras del Transporte”. Madrid: Sociedad Española de Mecánica del Suelo e Ingeniería Geotécnica, DL2000, pp. 843-859.

Alonso, E., Olivella, S., Pinyol, N. (2005). “A review of Beliche dam”. *Géotechnique*, Vol. 55, Issue 4, pp. 267-285.

Alonso, E., Cardoso, R. (2010). “Behaviour of materials for earth and rockfill dams: Perspective from unsaturated soil mechanics”. *Frontiers of Architecture and Civil Engineering in China*, Vol. 4, pp. 1-39.

Alonso, E., Tapias, M. (2019). “Suction and time effects in rockfill deformation”. *International Journal for Numerical and Analytical Methods in Geomechanics*, Vol. 43, pp. 1032-1050.

Atkinson, B. (1984). “Subcritical crack growth in geological materials”. *Journal of Geophysical Research*, Vol. 89, Issue B6, pp. 4077-4114.

Bauer, E. (2019). “Constitutive Modelling of Wetting Deformation of Rockfill Materials”. *International Journal of Civil Engineering*, Vol. 17, pp.481-486.

Broek, D. (1986). “Elementary engineering fracture mechanics”. Dordrecht: Martinus Nijhoff.

Cenor Consulting Engineers (2010a). “Somincor – Reservatório Cerro da Mina – Projecto de execução – Perfis transversais. Pormenores.”

Cenor Consulting Engineers (2010b). “Somincor – Reservatório Cerro da Mina – Projecto de execução – Planta de localização dos dispositivos de observação.”

Cenor Consulting Engineers (2010c). “Somincor – Reservatório Cerro da Mina – Projecto de execução – Planta geral da obra. Implantação.”

Cenor Consulting Engineers (2010d). “Somincor – Reservatório Cerro da Mina – Projecto de execução – Reservatório. Cortes transversais (1/2).”

Cenor Consulting Engineers (2010e). “Somincor. Reservatório Cerro da Mina – Volume I - Projecto de execução. Tomo I.3 – Estudo Geológico-Geotécnico.”

Cenor Consulting Engineers (2011). “Somincor. Reservatório Cerro da Mina – Volume V – Plano de observação e primeiro enchimento.”

Cetin, H., Laman, M., Ertunc, A. (2000). “Settlement and slaking problems in the world’s fourth largest rock-fill dam, the Ataturk Dam in Turkey”. *Engineering Geology*, Vol. 56, Issues 3-4, pp. 225-242.

Charles J A, Watts K S (1980). The influence of confining pressure on the shear strength of compacted rockfill. *Géotechnique*, Vol. 30, Issue 4, pp. 353-367.

Charles, J. (1990). “Laboratory compression tests and the deformation of rockfill structures”. In Maranhã das Neves, E. “Advances in rockfill structures”. Lisboa.

Charles, R. (1958). “Static fatigue of glass”. *Journal of Applied Physics*, Vol. 29, Issue 11, pp. 1549-1560.

Chávez, C., Romero, E., Alonso, E. (2009). “A rockfill triaxial cell with suction control”. *Geotechnical Testing Journal*, Vol. 32, Issue 3, pp. 1-13.

Clements, R. (1981). “The deformation of rockfill : inter-particle behaviour, bulk properties and behaviour in dams”. Dissertation of the Doctoral Degree, King's College.

De Mello, V. (1977). “Seventh Rankine Lecture: Reflections on design decisions of practical significance to embankment dams”. *Géotechnique*, Vol. 27, Issue 3, pp. 281-355.

Dolezalova, M., Hladik, I. (2008). “Constitutive Models for Simulation of Field Performance of Dams”. The 12th International Conference of the International Association for Computer Methods and Advances in Geomechanics, pp. 779-788.

-
- Dolzyk-Szypcio, K. (2019). “Stress-Dilatancy of Rounded and Angular Rockfill Materials”. World Multidisciplinary Earth Sciences Symposium (WMESS 2018).
- European Committee for Standardization (2006). “Natural stone test methods. Determination of real density and apparent density, and of total and open porosity”. NP-EN 1936, Instituto Português da Qualidade.
- Fell, R., MacGregor, P., Stapledon, D., Bell, G., Foster, M. (2015). “Geotechnical Engineering of Dams”. 2nd edition. CRC Press/Balkema.
- Ferreira, G. Tavares, G., Lopes, I., Brito, J., Romeiro, M., Oliveira, M., Rodrigues, A. (2018). “Monitoring and behaviour assessment of the Cerro do Lobo Tailings Dam and Cerro da Mina Reservoir of Somincor’s Neves-Corvo Mine”. 16^o Congresso Nacional de Geotecnia, Lisboa.
- Freiman, S. (1984). “Effects of chemical environments on slow crack growth in glasses and ceramics”. *Journal of Geophysical Research*, Vol. 89, Issue B6, pp. 4072-4076.
- Frossard, E., Hu, W., Dano, C., Hicher, P. (2012). “Rockfill shear strength evaluation: a rational method based on size effects”. *Géotechnique*, Vol. 62, Issue 5, pp. 415-427.
- Gallipoli, D., Gens, A., Sharma, R., Vaunat, J. (2003). “An elastoplastic model for unsaturated soil incorporating the effects of suction and degree of saturation on mechanical behaviour”. *Géotechnique*, Vol. 53, Issue 1, pp. 123-135.
- Hunter, G., Fell, R. (2003). “Rockfill Modulus and Settlement of Concrete Face Rockfill Dams”. *Journal of Geotechnical and Geoenvironmental Engineering*, Vol.129, Issue 10, pp. 909-917.
- Justo, J. (1990). “Collapse: its importance, fundamentals and modelling”. In Maranha das Neves, E. “Advances in rockfill structures”. Lisboa.
- Justo, J., Duran, P. (2000). “Settlement-time behaviour of granular embankments”. *International Journal for numerical and analytical methods in geomechanics*, Volume 24, Issue 3, pp. 281-303.
- Kermani, M., Konrad, J., Smith, M. (2017). “An empirical method for predicting post-construction settlement of concrete face rockfill dams”. *Canadian Geotechnical Journal*, Vol. 54, Issue 6, pp. 755-767.

-
- Kermani, M. (2016). "Prediction of post-construction settlements of rockfill dams, based on construction field data". Dissertation of the Doctoral Degree, Université Laval.
- Kovacevic, N. (1994). "Numerical analyses of rockfill dams, cut slopes and road embankments". Dissertation of the Doctoral Degree, Imperial College of Science, Technology and Medicine.
- Kutzner, C. (1997). "Earth and rockfill dams. Principles of design and construction". 1st edition. A. A. Balkema Publishers.
- Marcelino Silva, J. (1996). "Modelação do colapso e da fluência em aterros". Dissertation of the Doctoral Degree, Universidade do Porto.
- Marsal, R. (1967). "Large scale testing of rockfill materials". Journal of the Soil Mechanics and Foundation Division, ASCE, Vol. 93, Issue 2, pp. 27-43.
- Murakami, Y. (1987). "Stress intensity factors handbook". Oxford: Pergamon Press.
- Naylor, D., Maranha das Neves, E., Mattar, D., Veiga Pinto, A. (1986). "Prediction of construction performance of Beliche Dam". Géotechnique, Vol. 36, Issue 3, pp. 359-376.
- Nobari, E., Duncan, J. (1972). "Effect of reservoir filling on stresses and movements in earth and rockfill dams". Report No. TE-72-1. Department of Civil Engineering, University of California.
- Oldecop, L., Alonso, E. (2001). "A model for rockfill compressibility". Géotechnique; Vol. 51, Issue 2, pp. 127-139.
- Oldecop, L., Alonso, E. (2003). "Suction effects on rockfill compressibility". Géotechnique, Vol. 53, Issue 2, pp. 289-292.
- Oldecop, L., Alonso, E. (2004). "Testing rockfill under relative humidity control". Geotechnical Testing Journal; Vol. 27, Issue 3, pp. 269-278.
- Oldecop, L., Alonso, E. (2007). "Theoretical investigation of the time-dependent behaviour of rockfill". Géotechnique, Vol. 57, Issue 9, pp. 289-301.
- Ortega, E. (2008). "Comportamiento de materiales granulares gruesos – efecto de la succión". Technical University of Catalonia. In: UPC. Spain: Barcelona; 2008.
-

-
- Tada, H., Paris, P., Irwin, G. (1985). "The stress analysis of cracks handbook", 2nd ed. St Louis, MO: Paris Productions.
- Tapias, M., Alonso, E., Gili, J. (2015). "A particle model for rockfill behaviour". *Géotechnique*, Vol. 65, Issue 12, pp. 975-994.
- Tavares, G., Mateus de Brito, J., Romeiro, M., Lourenço, J., Oliveira, M. (2011). "Design of the Cerro da Mina Reservoir at the SOMINCOR's Neves Corvo Mine (Portugal)". 6th International Conference on Dam Engineering. C. Pina, E. Portela, J. Gomes (ed.), Lisboa.
- Tavares, G., Mateus de Brito, J., Romeiro, M., Oliveira, M. (2015). "Cerro da Mina Reservoir for industrial water. Main aspects of the design and construction".
- Teixeira Duarte Engenharia e Construções S.A. (2010). "Somincor – Reservatório Cerro da Mina – Relatório Final".
- Terzaghi, K. (1960). "Discussion on salt springs and lower bear riverdams". *Transactions of ASCE*, Vol. 125, Issue 2, pp. 139-148.
- USBR – Bureau of Reclamation, United States Department of the Interior (1987). "Design of smalls dams – A Water Resources Technical Publication". 3rd edition. U.S. Government Printing Office.
- Varadarajan, A., Sharma, K., Abbas, S., Dhawan, A. (2006). "Constitutive Model for Rockfill Materials and Determination of Material Constants". *International Journal of Geomechanics* Vol. 6, pp. 226-237.
- Wiederhorn, S., Freiman, S., Fuller, E., Simmons, C. (1982). "Effects of water and other dielectrics on crack growth". *Journal of Material Science*, Vol. 17, pp. 3460-3478.
- Wilson, S., Marsal, R. (1979). "Current Trends in Design and Construction of Embankment Dams". ASCE, New York, USA.
- Xiao, L., Liu, H. (2017). "Elastoplastic Constitutive Model for Rockfill Materials Considering Particle Breakage". *International Journal of Geomechanics*, Vol. 17, Issue 1, 04016041.1-04016041.13.